Quarterly Reviews of Biophysics

www.cambridge.org/qrb

Some general principles of riboswitch structure and interactions with small-molecule ligands

Lin Huang[1] and David M. J. Lilley[2]

[1]Guangdong Provincial Key Laboratory of Malignant Tumor Epigenetics and Gene Regulation, Guangdong-Hong Kong Joint Laboratory for RNA Medicine, Medical Research Center, Sun Yat-Sen Memorial Hospital, Sun Yat-Sen University, Guangzhou 510120, China and [2]Molecular, Cellular and Developmental Biology Division, School of Life Sciences, University of Dundee, Dundee DD1 5EH, UK

Review

Cite this article: Huang L and Lilley DMJ (2025). Some general principles of riboswitch structure and interactions with small-molecule ligands. *Quarterly Reviews of Biophysics*, **58**, e13, 1–22
https://doi.org/10.1017/S0033583525100012

Received: 26 February 2025
Revised: 24 April 2025
Accepted: 25 April 2025

Keywords:
biomolecular systems; crystallography; RNA; structural biology; ligand binding

Corresponding author:
David M. J. Lilley;
Email: d.m.j.lilley@dundee.ac.uk

Abstract

Riboswitches are RNA elements with a defined structure found in noncoding sections of genes that allow the direct control of gene expression by the binding of small molecules functionally related to the gene product. In most cases, this is a metabolite in the same (typically biosynthetic) pathway as an enzyme (or transporter) encoded by the gene that is controlled. The structures of many riboswitches have been determined and this provides a large database of RNA structure and ligand binding. In this review, we extract general principles of RNA structure and the manner or ligand binding from this resource.

Table of contents

General introduction to riboswitches

Riboswitches are RNA elements with a defined structure found in noncoding sections of genes that allow the direct control of gene expression by the binding of small molecules functionally related to the gene product. In most cases, this is a metabolite in the same (typically biosynthetic) pathway as an enzyme (or transporter) encoded by the gene that is controlled. Riboswitches allow the sensing of the concentration of a small molecule and switch the level of expression of the gene product at a particular threshold. Most riboswitches affect their genetic control either at the transcriptional level (where ligand binding can affect the relative stability of terminator or anti-terminator stem-loop structures for example) or at the translational level (where the RNA structure modulates the accessibility of the ribosome binding site). The riboswitches could operate either as an OFF or ON switch, increasing or decreasing the level of expression. For biosynthesis, expression needs to be turned off when the concentration of the metabolite has reached the required level. On the other hand, a transporter that is required to export a toxic metabolite (e.g., guanidine) would only be required when that compound has exceeded a predetermined level.

In principle, RNA folding might attain equilibrium with the ligand (thermodynamic control), or the ligand might bind folding intermediates during co-transcriptional folding (kinetic control). Early studies indicated that RNA folding led to a limited time during which ligand binding competed with continued transcription, that is, kinetic control (Wickiser et al., 2005; Lemay et al., 2006), and this has been supported by more recent studies, at least in transcriptionally controlled riboswitches (Frieda and Block, 2012; Widom et al., 2018; Hua et al., 2020).

From the first discussions of riboswitches, the RNA was described in terms of two domains: the aptamer domain (that binds the ligand) and the expression domain that modulate gene expression, for example, by the formation of a transcriptional terminator. However, this may be more applicable to some riboswitches than others, and as we discuss below may not be appropriate for many translational riboswitches. The regulation of gene expression by riboswitches appears to be a largely prokaryotic phenomenon. Exceptions to this include the thiamine pyrophosphate (TPP) riboswitches found in fungi and plants (Winkler et al., 2002), where they control splicing (Cheah et al., 2007), and an archaeal fluoride riboswitch (Baker et al., 2012). Perhaps other eukaryotic riboswitches await discovery.

There are over 55 riboswitch classes, sensing a diverse group of metabolites. These include coenzymes (such as SAM, TPP, NAD^+, FMN); sugars (e.g., glucosamine-6-phosphate); elements of RNA (nucleobases, PRPP, etc.) and RNA derivatives (e.g., xanthine, preQ$_1$); amino acids (e.g., glycine, glutamine); signaling molecules (e.g., cyclic AMP-GMP, cyclic diGMP, etc.); and even simple ions (cations like magnesium or anions like fluoride). Many of these have been discovered in the Breaker laboratory (Breaker, 2012; McCown et al., 2017; Kavita and Breaker, 2023) using bioinformatics to identify structured inter-genic regions in RNA sequences. In many cases, a given ligand can be sensed by multiple riboswitches with different structures, modes of ligand binding, and, in some cases, different mechanisms of gene regulation. For example, there are six SAM-sensing riboswitches (seven if the SAM–S-adenosylhomocysteine [SAH] riboswitch is included).

Although according to their strict definition riboswitches are regulatory elements that respond to a small-molecule ligand, there are *cis*-acting elements that act in the same way in response to larger molecules, such as tRNA (Henkin et al., 1992; Zhang and Ferre-D'amare, 2013). The synthesis of the k-turn-binding protein L7Ae is subject to autoregulation by the binding of archaeal L7Ae to an element located in the 5′-UTR of its mRNA (Daume et al., 2017), so stabilizing a k-turn-containing stem-loop and thereby preventing access to the ribosome binding site (Huang et al., 2019a). In all respects other than the size of the ligand, this operates as a riboswitch.

We do not intend to survey the occurrence and function of riboswitches comprehensively here; there are several excellent reviews that do that (Kavita and Breaker, 2023; Olenginski et al., 2024). This is also surveyed in the web-based database https://riboswitch.ribocentre.org/riboswitches/ (Bu et al., 2024). Rather, this review is written from our own structural perspective, and focuses on what can be learned from the large numbers of structures of riboswitches, as a valuable database of RNA structure and ligand binding to RNA.

Architectural principals of riboswitch structure

Riboswitches are autonomously folding sections of RNA that create small-molecule ligand binding sites. The structures of the majority of riboswitches have been determined at good resolution. The ensemble of these structures provides a rich source of structural data on RNA architecture.

Global structural architecture of riboswitches

In general, the majority of riboswitches are relatively small (typically between 50 and 80 nucleotides in length), and their architectures are often based around a single structural feature. These can be classified as helical junctions, pseudoknots (PKs), and loop–loop interactions. Moreover, these elements usually create the binding sites for the riboswitch ligands. In general, the helical junctions determine the trajectory of the helical arms, and contacts between them may be facilitated.

Helical junctions

Helical junctions are the association of multiple helical sections, connected through the exchange of covalently continuous strands, and can be classified according to a formal nomenclature (Lilley et al., 1995) (Figure 1). The most common junctions have three or four helical arms. These can be perfectly base paired (e.g., a 4H four-way junction has no unpaired nucleotides at the point of strand exchange between the helices), or they can have additional nucleotides on one or more sections that connect the helical arms (Figure 1a). There is a strong tendency for helical arms to undergo pairwise coaxial stacking, and junctions generally fold into a structure that maximizes stacking. The conformation of any junction can be influenced by additional tertiary contacts between remote elements within the helical arms; this is a very common occurrence in junctions found in riboswitches.

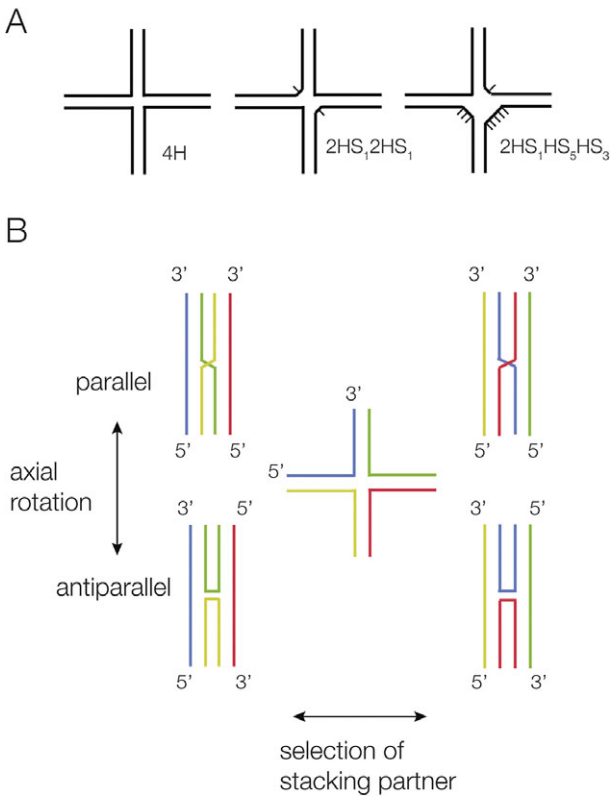

Figure 1. Scheme showing the nomenclature for four-way helical junctions, and their stacking conformations. (A) Junctions can vary according to the number of unpaired nucleotides between helical sections. A 4H junction has no unpaired nucleotides, whereas the 2HS$_1$2HS$_1$ junction has two one-nucleotide single-strand sections diametrically opposed. These junctions are named according to the IUPAC nomenclature (Lilley et al., 1995). (B) Two conformers are possible when four-way junctions undergo pairwise coaxial stacking (left and right). The structures can rotate about their centers, forming parallel or antiparallel structures in the extreme (upper and lower). In the parallel structures, the continuous strands run in the same direction, and the exchanging strands cross.

https://doi.org/10.1017/S0033583525100012 Published online by Cambridge University Press

Four-way helical junctions A four-way junction with pairwise coaxial stacking of helical arms can adopt two possible conformers depending on the selection of stacking partners, and the coaxial pairs can adopt either parallel or antiparallel conformations (Figure 1b). Perfect four-way junctions in RNA are more structurally polymorphic than their DNA equivalents (Duckett et al., 1995; Hohng et al., 2004). DNA 4H junctions always adopt an antiparallel geometry (Duckett et al., 1988; Murchie et al., 1989), and in the absence of branch migration, the only dynamic mode is the exchange of stacking conformers (McKinney et al., 2003). By contrast, RNA 4H junctions can adopt both parallel and antiparallel conformations (Duckett et al., 1995), with the parallel geometry being more stable in most cases. Single-molecule FRET analysis has shown that a given junction can be quite dynamic in free solution, exchanging between parallel and antiparallel conformations as well as between stacking conformers (Hohng et al., 2004). If elements within the helical arms that are separated from the junction can interact (e.g., a loop–receptor interaction), this will naturally influence the angle between the axes between the coaxial pairs, and thus the geometry of the junction.

The NiCo (Furukawa et al., 2015), yybP-ykoY manganese (Dambach et al., 2015), and PRPP (Nelson et al., 2017) riboswitches each contain a parallel four-way junction. The manganese riboswitch contains a perfect 4H junction (no unpaired additional nucleotides), with near-perfect pairwise coaxial stacking between the helical arms and within 20° of having parallel axes (Price et al., 2015) (Figure 2). Two of the helical arms interact via a loop extended from one of them, and this likely is responsible for the near side-by-side geometry of the helical arms. In contrast to the manganese riboswitch junction, the four-way helical junctions of the NiCo (Furukawa et al., 2015) and PRPP riboswitches are not 4H junctions, but have a number of nucleotides within the sections that connect the helical arms. Despite this, the overall geometry of the junctions remains quite similar, and both adopt a parallel geometry. The NiCo riboswitch four-way junction (Furukawa et al., 2015) has one extra nucleotide at the point of strand exchange on each of the exchanging strands. The junction is parallel, and the pairwise coaxial stacking across the exchange point is good, with the nucleobases spaced by ~3 Å for both. The PRPP riboswitch junction has more unpaired nucleotides, making a $2HS_1HS_5HS_3$ junction (Knappenberger et al., 2018). Two of the helices are perfectly coaxially stacked, with full base pairing and with the nucleobases spaced by 3.3 Å. In contrast, the other pair is separated by what is effectively an internal loop (five and three nucleotides on the two strands) and so that the helices are not truly coaxial. This loop forms the ligand binding site. The kinking directs one of the helices so that its terminal loop forms a terminal loop–internal loop interaction with the longer helix of the well-stacked pair.

Three-way helical junctions Three-way junctions are the most common helical junctions found in riboswitches, and have been analyzed in terms of their preferred structural conformers (Lescoute and Westhof, 2006; Ouellet et al., 2010). The majority of three-way RNA junctions have additional nucleotides in the sections linking the helices; 3H junctions are very rare in RNA. As with four-way junctions, there is a strong tendency for three-way junctions to undergo pairwise coaxial stacking of helices, but with an odd number of helical arms, only two of the three can undergo coaxial stacking, and in general, a single stacking conformer is observed as the most stable. This is normally one that minimizes the number of unpaired nucleotides on the connecting strand. There are then two types of connection possible, according to whether the longest connecting section passes 5′ to 3′ from the coaxially stacked helices into the third helix (L_{ex}) or from the third helix into the stacked pair of helices (L_{en}) (Ouellet et al., 2010) (Figure 3).

Three-way junctions form the central structural motif of numerous riboswitches, including SAM-III (Lu et al., 2008), tetrahydrofolate (THF) (Trausch et al., 2011), TPP (Thore et al., 2006), 2′-deoxyguanosine-I (2′-dG-I) (Pikovskaya et al., 2011), 3′,3’-cGAMP (Ren et al., 2015a), magnesium ion (Ramesh et al., 2011), glutamine-I

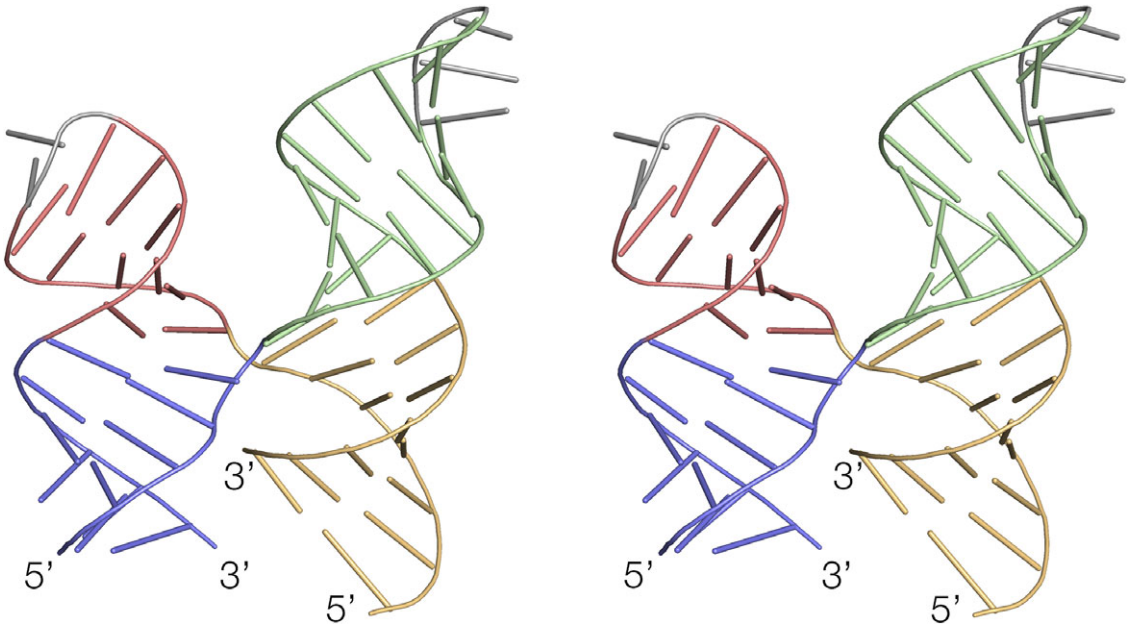

Figure 2. The four-way RNA junction of the magnesium riboswitch (Price et al., 2015). This is a perfect 4H junction that adopts a parallel conformation. The structure is shown as a parallel-eye stereoscopic view (PDB ID 4YLI).

https://doi.org/10.1017/S0033583525100012 Published online by Cambridge University Press

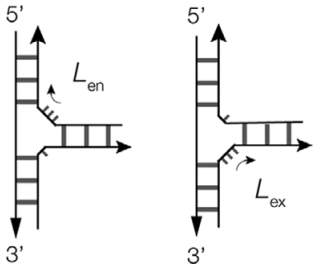

Figure 3. Scheme showing the possible conformations of three-way RNA junctions. The most stable conformer is generally the one that minimizes the number of unpaired nucleotides on the connecting strand. Two conformations are possible, that differ in the direction of the longest connecting section. We have defined these as L_{ex} or L_{en}, depending on whether the longest connecting section passes from the coaxially stacked helices into or out of the third helix (L_{ex}), the third helix, respectively (Ouellet et al., 2010).

(Ren et al., 2015b), glycine (Huang et al., 2010), adenine (Serganov et al., 2004), and guanine (Batey et al., 2004) riboswitches (Figure 4). While most exhibit coaxial pairwise helical stacking, some do not, such as the three-way junctions found in the SAM-III and 3′,3′-cGMP riboswitch. In the majority of three-way junctions, the additional nucleotides linking the helices make specific interactions within the core of the junction, such as a U:G.A triple in the THF riboswitch (Trausch et al., 2011). Frequently base stacking is preserved within the formally single-stranded regions, helping to maintain coaxial alignment between the helical arms. In many riboswitches, three-way junctions, the longest linking region (typically ≥5 nucleotides) forms a distinct turn, behaving as a pseudo-forth helical arm. In these cases (both L_{ex} and L_{en} conformations), there is a sharp turn close to the 5′ end of the single-stranded region, after which the nucleotides at the 3′ end are mutually stacked (Figure 5). Good examples are found in the glycine (Huang et al., 2010), THF (Trausch et al., 2011), and 2′-dG-I (Pikovskaya et al., 2011) riboswitches. The most extreme versions of this conformation are found in the adenine (Serganov et al., 2004) and guanine (Batey et al., 2004) riboswitches, where the linking section forms a complete turn terminated by a Watson–Crick G:C base pair (Figure 4c). Thus, these junctions are intermediate between three- and four-way helical junctions. The magnesium ion riboswitch contains two three-way junctions, where the third helix of the 5′ junction branches into the second junction, a $2HS_2HS_5$ junction that is in the L_{ex} conformation.

The three-way junctions of the TPP riboswitches (Serganov et al., 2006; Thore et al., 2006) adopt a distinct conformation termed a k-junction, which is a combination of a three-way junction and a k-turn (see Section entitled "k-turns and k-junctions") (Wang et al., 2014; Li et al., 2023). The k-junction has all the features of a k-turn (Klein et al., 2001; Goody et al., 2004; Huang and Lilley, 2016), including the tandem sheared G•A base pairs, the cross-strand hydrogen bonds, and the bulge, but with an additional helix (thus creating a three-way junction) where the two helical arms of the k-turn connect on the non-bulged strand (Figure 6). Upon folding by addition of metal ions, the k-junction, like the k-turn, introduces a sharp kink into the C and NC helices, with an included angle of close to 50° (Li et al., 2023). In the *Arabidopsis* and *Escherichia coli* TPP riboswitches (Serganov et al., 2006; Thore et al., 2006), the ligand binds into receptors formed between these helices, with a turn of helix remote from the junction. Although k-junctions were first identified in TPP riboswitches, they occur more widely and

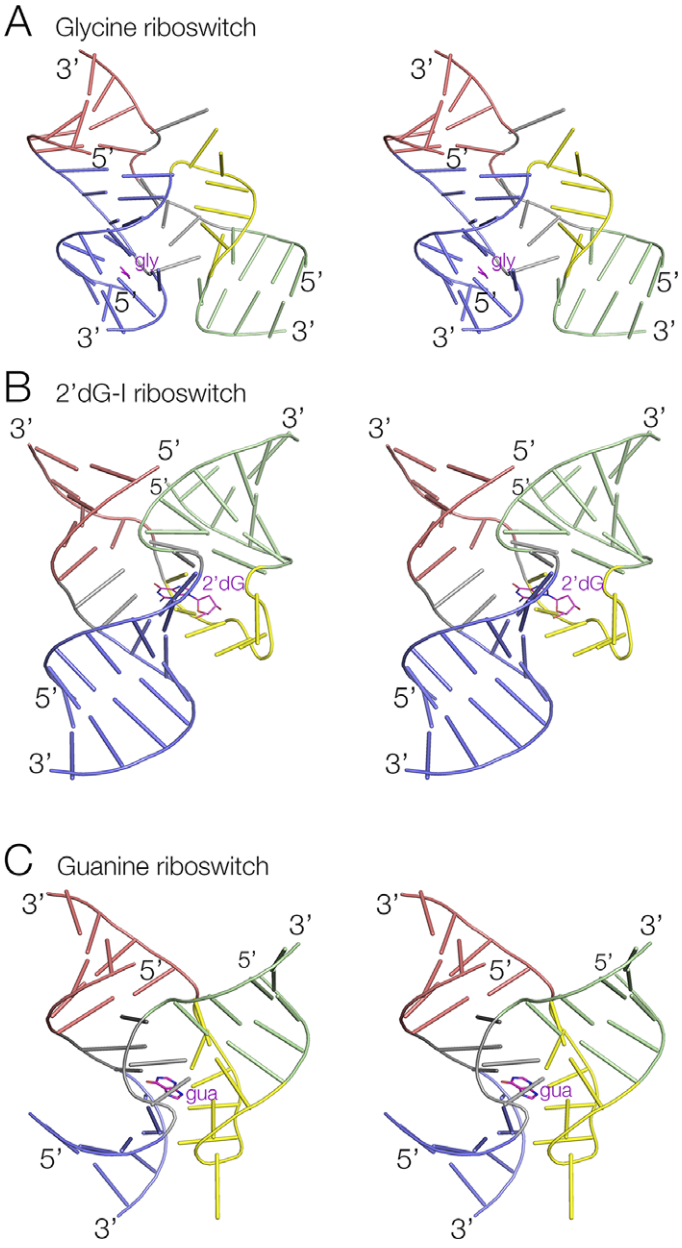

Figure 4. Three examples of three-way RNA junctions found in riboswitches. Parallel-eye stereoscopic views of the junctions found in (A) The glycine riboswitch (Huang et al., 2010) (PDB ID 3OWW). (B) The 2′-deoxyguanine-I riboswitch (Pikovskaya et al., 2011) (PDB ID 2SKI). (C) The guanine riboswitch (Batey et al., 2004) (PDB ID 4FE5). In each case, the long unpaired loop region of RNA is colored yellow. The ligands are colored magenta and named gly, 2′dG, and gua, respectively.

have been found in ribosomal RNA (Wang et al., 2014) and in RNA sequences of unknown function (Li et al., 2023).

Higher order helical junctions Helical junctions of a higher order than four are possible, although they would be expected to experience some steric clash. The structure of the lysine riboswitch (Grundy et al., 2003; Sudarsan et al., 2003) is based upon a five-way helical junction (Figure 7) (Garst et al., 2008; Serganov et al., 2008). Formally, the junction is $3HS_2HS_1HS_2$. The red, light green, pink, and blue helices form an antiparallel four-way junction in which the red and light green helices are perfectly coaxial. The fifth helix (dark green) is inserted at the center of the continuous strand linking the blue and pink helices. This is difficult to depict clearly in a two-dimensional

https://doi.org/10.1017/S0033583525100012 Published online by Cambridge University Press

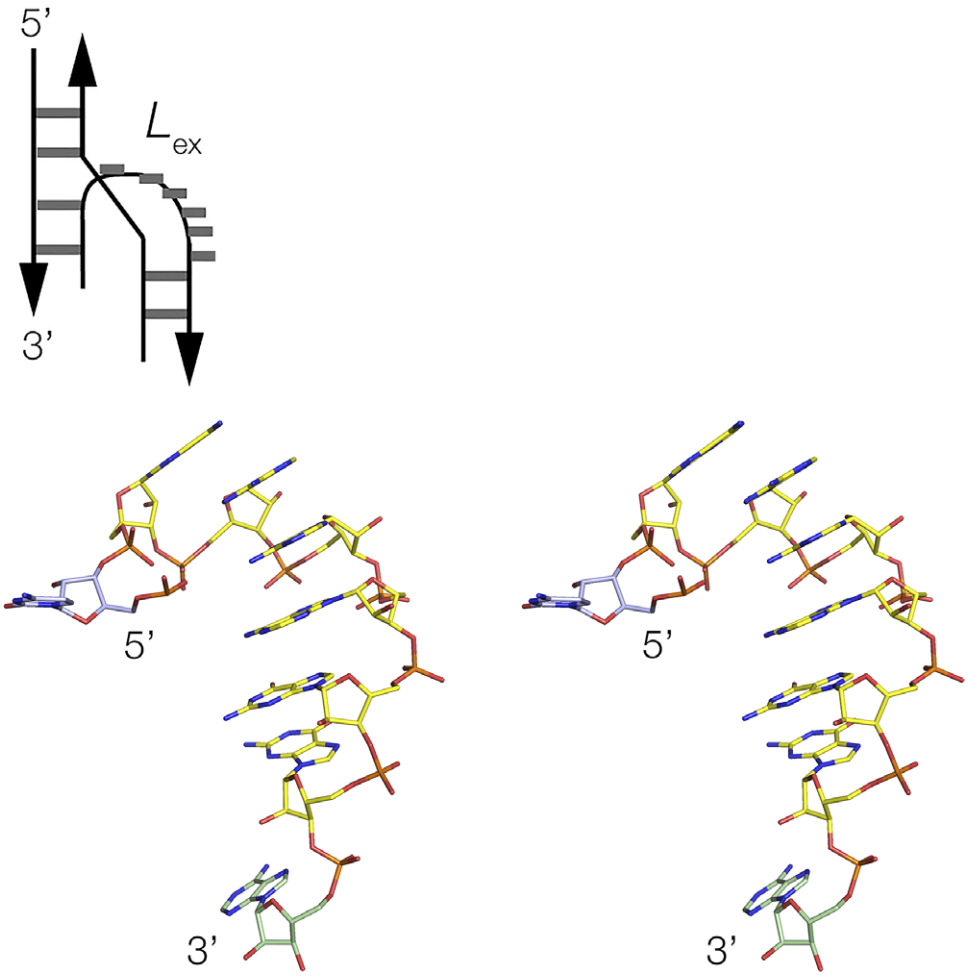

Figure 5. The unpaired loop of the glycine riboswitch (Huang et al., 2010) three-way junction is shown schematically (top) and as a parallel-eye stereoscopic view (bottom). This is a detail taken from the three-way junction shown in Figure 4a (PDB ID 3OWW).

image, but becomes significantly clearer when viewed in three dimensions. Interestingly, the lysine ligand is bound in the core of the five-way junction. The red, blue, and dark green helices form a three-helix bundle and are held together by loop–loop and loop–receptor interactions remote from the junction.

Pseudoknot-containing structures

The major structural feature of a number of riboswitches is a PK, including the three $PreQ_1$ riboswitches (Liberman et al., 2013; Connelly et al., 2019; Schroeder et al., 2023), SAM–SAH (Huang et al., 2020a), guanidine-III (Huang et al., 2017b), NAD^+-II (Peng et al., 2023; Xu et al., 2023), and GlmS (Cochrane et al., 2007; Klein and Ferré-D'amaré, 2006) riboswitches. The simplest form of PK is where the terminal loop of a stem-loop structure forms a helix with a remote complementary strand. The standard H-type PK structure (Figure 8) includes two such interactions formed from two inverted repeat sequences, each forming stem-loops such that the loop of each contains one strand of the stem of the other. The remaining part of the loop then acts as a linker. In general, the linker aligns with the major groove of the helix with an open 3′ end, while the other linker aligns with the minor groove of the helix with an open 5′ end. The basic PK structure can then be elaborated by the inclusion of additional helices.

Some examples of riboswitch PK structures are shown in Figure 9. The organization and crystal structure of the SAM/SAH riboswitch are shown in Figure 9a. This is a standard H-type PK, although it was constructed from two RNA oligonucleotides so that the 11 nt linker connecting the two helices was omitted (Huang et al., 2020a). The two helices are coaxial, and the linker lies in the major groove of the helix with an open 3′ end, making one triple interaction. The guanidine-III riboswitch is another standard H-type PK, and the complete structure is visible in the crystal structure (Figure 9b) (Huang et al., 2017b). One linking segment lies in the major groove of the 3′ end helix and makes a series of triple interactions (see below), while the other is on the minor groove side of the 5′ end helix and makes fewer interactions. The $PreQ_1$ riboswitches are all based upon a PK structure. The structure of the $PreQ_1$-III riboswitch PK (Schroeder et al., 2023) is shown in Figure 9c. Like that of the $PreQ_1$-II riboswitch (Liberman et al., 2013), the PK is elaborated by an additional helix within a linking segment connecting the 3′ end helix. The NAD^+-II riboswitch is based upon perhaps the most complicated structure, shown in Figure 9d (Peng et al., 2023). The structure is an H-type PK with an additional helix inserted into the central linker that connects the two helices. It is further elaborated by two successive four-nucleotide interactions in the central region. Finally, the GlmS

https://doi.org/10.1017/S0033583525100012 Published online by Cambridge University Press

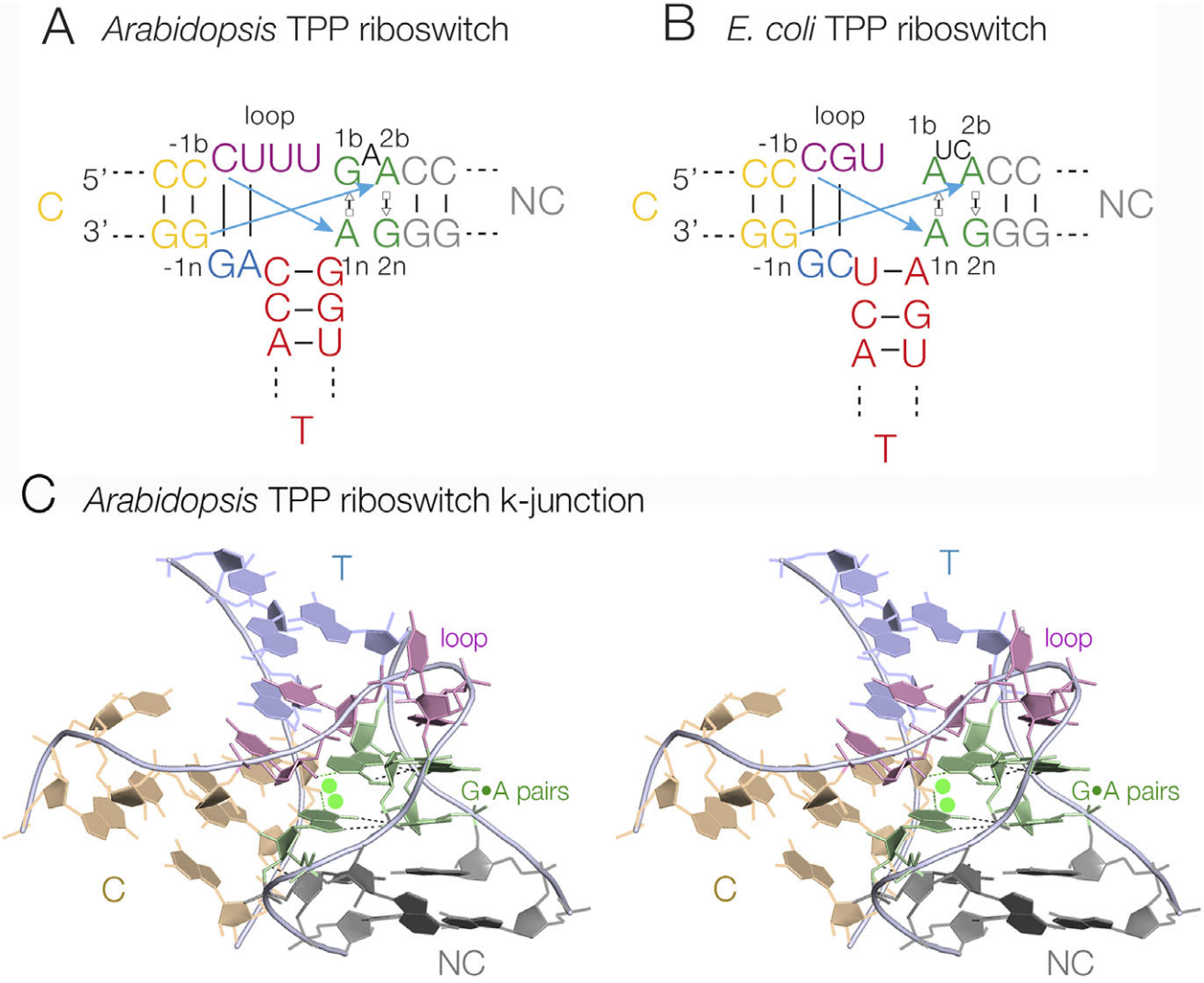

Figure 6. k-Junctions found in TPP riboswitches. (A) The sequence of the *Arabidopsis thaliana* TPP riboswitch. (B) The sequence of the *E. coli* TPP riboswitch. The standard cross-strand k-turn hydrogen bonds are indicated by the cyan arrows. (C) The crystal structure of the *A. thaliana* TPP riboswitch (Thore et al., 2006) k-junction shown in parallel-eye stereoscopic view (PDB ID 3D2G).

riboswitch, which has ribozyme activity mediated by its glucosamine-6-phosphate ligand (Winkler et al., 2004), is based upon a secondary structure with multiple PK structures (Cochrane et al., 2007; Klein and Ferré-D'amaré, 2006).

Loop–loop interacting structures

An interaction between two terminal loops is the principal structure feature in some riboswitches that creates the specific ligand binding site. Perhaps, the best example of this is the guanidine-II riboswitch (Sherlock et al., 2017). This comprises two stem-loops of closely similar sequence connected by a short linker, and crystallographic studies have shown that the individual stem-loops dimerize in the crystal by an intimate interaction between the loops (Huang et al., 2017a; Reiss and Strobel, 2017) (Figure 10). The loop–loop interaction comprises the formation of two regular C:G base pairs, a triple interaction between the terminal C:G base pair of the loop and N1 and N6 of the 5′ adenine of the loop, and a stacking interaction between the two 3′ adenine nucleobases of the loop. The loop–loop interaction creates two symmetrically related guanidine binding sites, and the guanidine molecules contribute to the stability of the loop–loop interaction; this is discussed further below.

Another riboswitch that can be considered to be based on two interacting loops is the glutamine-II riboswitch (Ames and Breaker, 2011), although semantically this might also be termed a kind of PK. The interface comprises six consecutive Watson–Crick base pairs with two major-groove triple base interactions (Huang et al., 2019b). The L-glutamine ligand is bound on the major-groove face of the terminal loop. The lysine riboswitch has a loop–loop interaction comprising six uninterrupted Watson–Crick base pairs (Garst et al., 2008; Serganov et al., 2008). This is important in achieving the overall fold of the RNA, but is not directly involved in the binding of the lysine ligand.

Local structural elements of riboswitches

Loop–loop and loop–receptor interactions

The guanidine-binding domain of the guanidine-II riboswitch is fundamentally based upon a loop–loop interaction between two stem-loops that is mediated by ligand binding. This is discussed in

https://doi.org/10.1017/S0033583525100012 Published online by Cambridge University Press

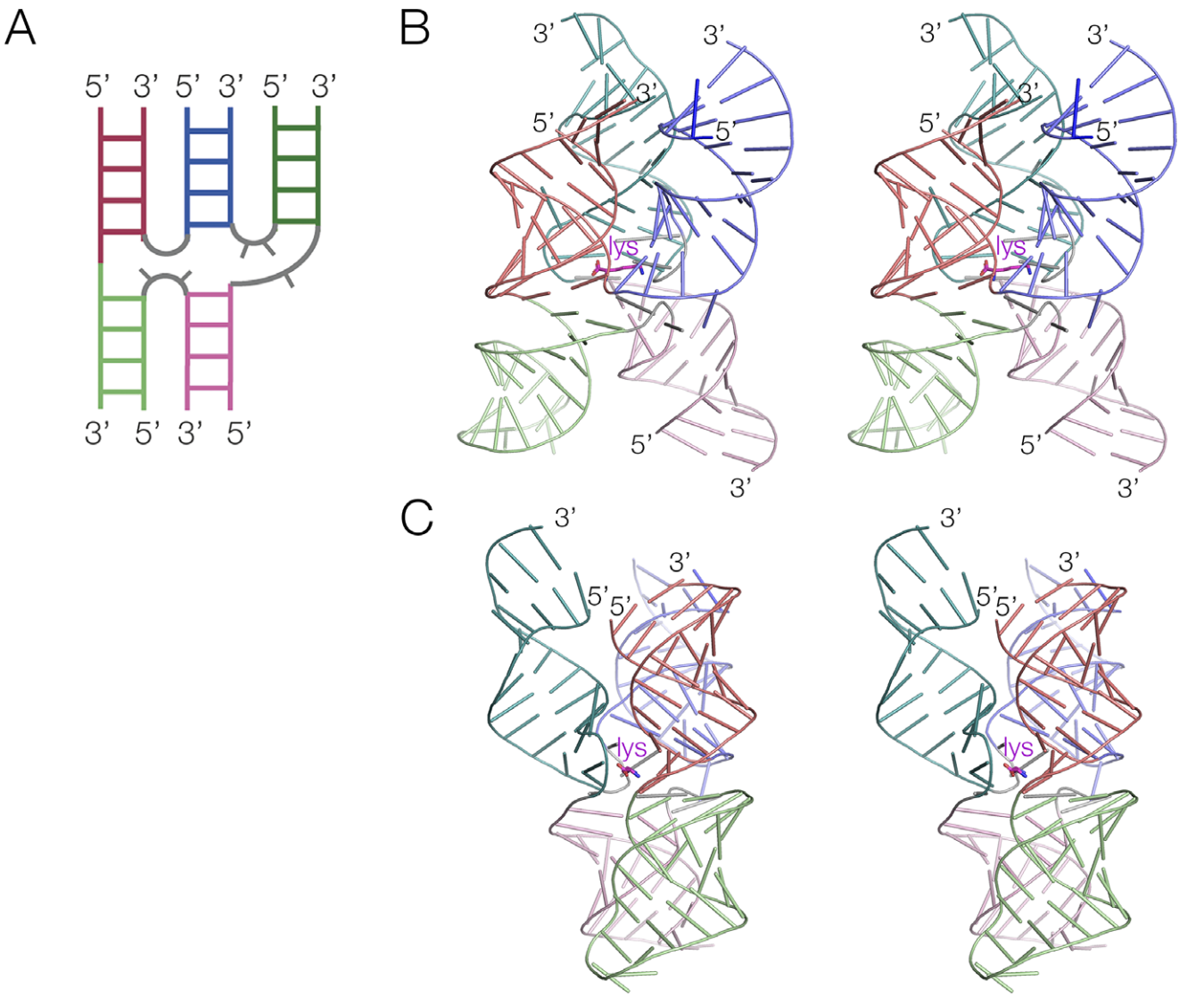

Figure 7. A five-way junction found in the *Thermotoga maritima* lysine riboswitch (Garst et al., 2008). (A) Schematic showing the connectivity of the five-way RNA junction. (B) Front and *Conura side* views of the structure of the five-way junction shown in parallel-eye stereoscopic view (PDB ID 3DIL).

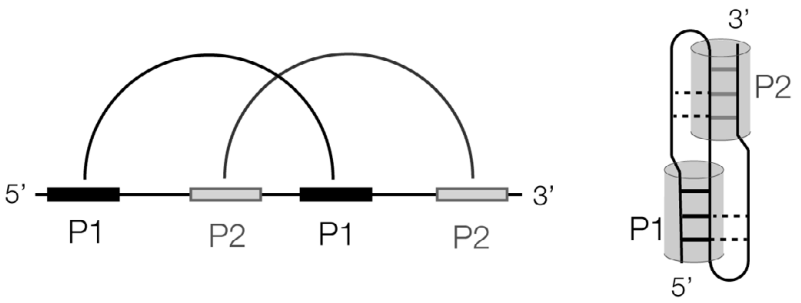

Figure 8. Scheme showing the formation of an H-type pseudoknot structure. In the linear form (left) paired regions are connected by the arcs. A cartoon of the folded form is shown (right) with the P1 and P2 helices shown as cylinders.

the previous section, and is shown in Figure 10. Loop–loop interaction also occurs in the lysine riboswitch (Garst et al., 2008) and the various purine-binding riboswitches (Batey et al., 2004; Serganov et al., 2004). Loop–receptor interactions are very common in folded RNA species, so unsurprisingly they occur in several riboswitches. Such interactions are structurally important in the guanidine-I riboswitch (Reiss et al., 2017), the TPP riboswitch (Thore et al., 2006), and the THF riboswitch (Trausch et al., 2011).

https://doi.org/10.1017/S0033583525100012 Published online by Cambridge University Press

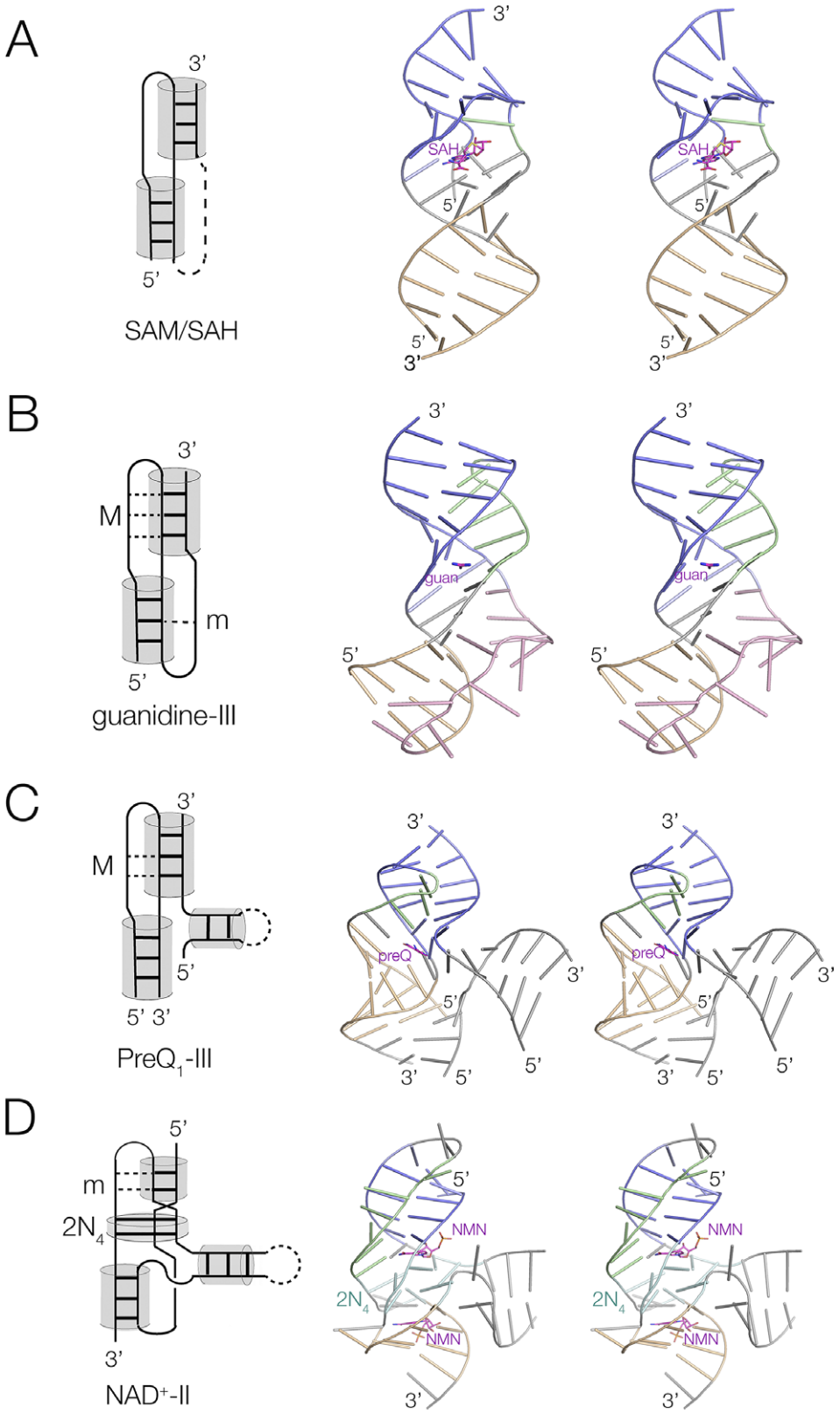

Figure 9. Representative examples of ribozymes with structures that are based on pseudoknots. Each is shown as the schematic of the folded structure (left), and a cartoon representation of the three-dimensional structure shown in parallel-eye stereoscopic view (right). (A) The SAM/SAH riboswitch (Huang et al., 2020a) (PDB ID 6YL5). (B) The guanidine-III riboswitch (Huang et al., 2017b) (PDB ID 5NWQ). (C) The $PreQ_1$-III riboswitch (Schroeder et al., 2023) (PDB ID 6XKO). (D) The NAD^+-II riboswitch (Peng et al., 2023) (PDB ID 8HB8).

https://doi.org/10.1017/S0033583525100012 Published online by Cambridge University Press

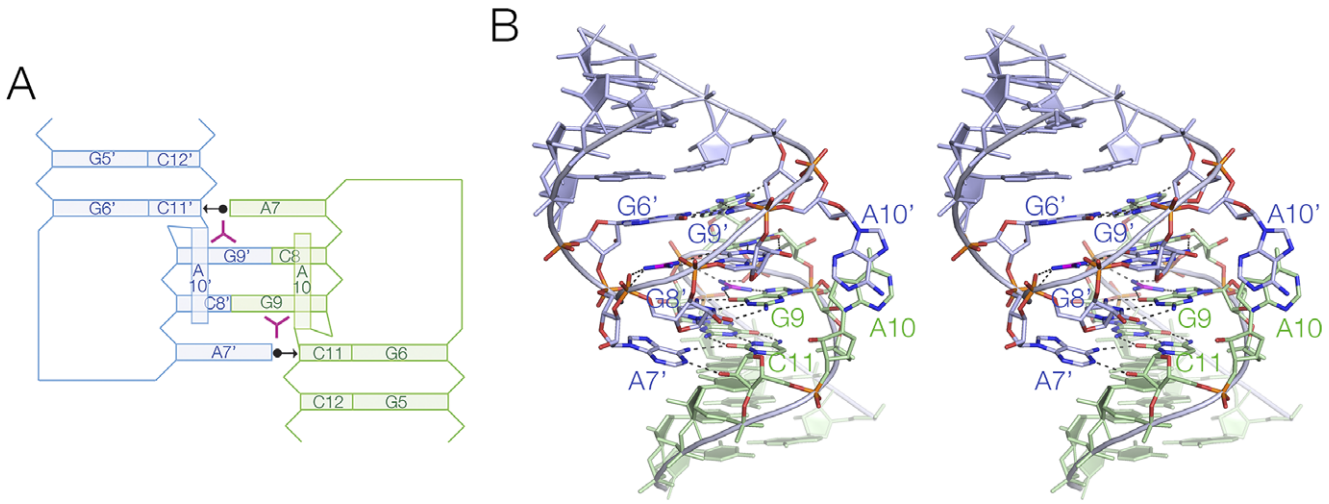

Figure 10. Loop–loop interaction in the guanidine-II riboswitch (Huang et al., 2017a). (A) Schematic showing the interaction between the two loops, colored blue and green. (B) The crystal structure of the loop–loop interaction shown in parallel-eye stereoscopic view (PDB ID 5NOM).

Triple helical regions

Triple helices are formed where a third strand locates in the major or minor groove of a duplex, making hydrogen bonding interactions with the nucleobases and perhaps the backbone. These are relatively common in riboswitches, including the preQ$_1$-III (Schroeder et al., 2023), guanidine-III (Huang et al., 2017b), SAM-II (Gilbert et al., 2008), SAM-V (Huang and Lilley, 2018b), and NAD$^+$-II (Peng et al., 2023; Xu et al., 2023) riboswitches. Riboswitches based upon PK structures will typically have a major groove triple helix, and in some cases, a minor groove triple helix too. In general, where the triple helix has an open 3′ end, this will form a major groove triplex. The guanidine-III riboswitch is an example, shown in Figure 11 (Huang et al., 2017b). The triple helix forms four planes of base triple interactions, where the three nucleobases are approximately co-planar, and stacked on both sides with a separation of about 3.5 Å. The sequence of the third strand is 5′ AGGU, and in each case, the nucleobases are hydrogen bonded to the Hoogsteen edge of one or both base pairs of the duplex. The nucleotide 5′ to the third strand of the duplex (G7) plays a key role in bonding the guanidine ligand as we discuss below.

As we have discussed above (see Figure 9b), the guanidine-III riboswitch forms a standard H-type PK, and the helix containing the 5′ end accommodates the connecting strand in its minor groove. However, this strand makes no triple-base interactions in the minor groove, and only two base pairs along its length, a *cis*-Watson–Crick and a *trans*-Watson–Crick base pair (Huang et al., 2017b). The sequence requirements for a regular minor-groove triple helix are more stringent and essentially require an oligo-adenine sequence that can form A-minor interactions (Nissen et al., 2001). The NAD$^+$-II riboswitch provides a good example of a minor groove triplex, where the third strand comprises five consecutive adenine nucleotides (A_5, comprising A41 to A45). The structure of the triple helix (Peng et al., 2023) is shown in Figure 12. Each adenine nucleobase makes hydrogen bonding interactions with the sugar edge of the base pairs of the duplex, either one or both nucleobases or the O2' of the sugar. Starting from the 3′ end of the A_5 sequence, the first three adenine nucleobases make hydrogen bonds from their Watson–Crick edge (N6, N1) to one or both nucleobases of the duplex plus an O2', and the forth (A42) is hydrogen bonded from its Hoogsteen edge (N6, N7) to the sugar O2' and nucleobase (cytosine O2) of the duplex. The final, that is, 5′ adenine (A41), is reoriented in making a turn, so that its sugar edge faces the duplex, whereupon it is hydrogen bonded to the nucleobase (guanine N2) and sugar (cytosine O2') of the duplex.

Tetraplex helices

While triple-base interactions have been found frequently in riboswitches, quadruple interactions are less common. Nevertheless, they exist. The NAD$^+$-II riboswitch has a section of quadruple helix comprising two successive quadruplexes G:U:A:C and U:A:A:G (Figure 13) (Peng et al., 2023). The nucleobases are all coplanar, and are connected by hydrogen bonding between successive nucleobases in a cyclic manner. The upper G:U:A:C plane forms a platform for the binding of the planar nicotinamide dinucleotide ligand. Base tetrads have also been found in purine riboswitches such as the 2′-dG-II riboswitch (Matyjasik and Batey, 2019). Base tetrads are relatively rare, and we are unaware of any examples of four-guanine tetraplex structures in riboswitches.

k-Turns and k-junctions

We have reviewed the structure and occurrence of kink turns (k-turns) at length previously (Huang and Lilley, 2018a). The motif is extremely widespread in RNA structure, being found in the ribosome (several examples) (Klein et al., 2001), spliceosomal complexes (Vidovic et al., 2000), and in snoRNA species such as box C/D (Moore et al., 2004). The standard k-turn comprises two successive sheared G•A and A•G base pairs preceded by a three-nucleotide bulge. When folded in the presence of divalent cations, the RNA is tightly kinked, and stabilized by two key cross-strand A-minor interactions (Liu and Lilley, 2007; McPhee et al., 2014; Huang et al., 2016). The folded structure of the k-turn can also be stabilized by protein binding, particularly by proteins of the L7Ae class (Turner and Lilley, 2008; Wang et al., 2012; Huang and Lilley, 2013). The SAM-I riboswitch contains a standard k-turn within its architecture (Montange and Batey, 2006). It folds in response to the addition of divalent metal ions, and both folding and SAM binding are prevented by mutations that disrupt the standard A-minor interactions (Schroeder et al., 2011). k-Turns also exist in the glycine (Baird and Ferre-D'amare, 2013), lysine (Blouin and Lafontaine, 2007), cobalamine (Johnson Jr et al., 2012), and cyclic diGMP (Smith et al., 2009) riboswitches.

https://doi.org/10.1017/S0033583525100012 Published online by Cambridge University Press

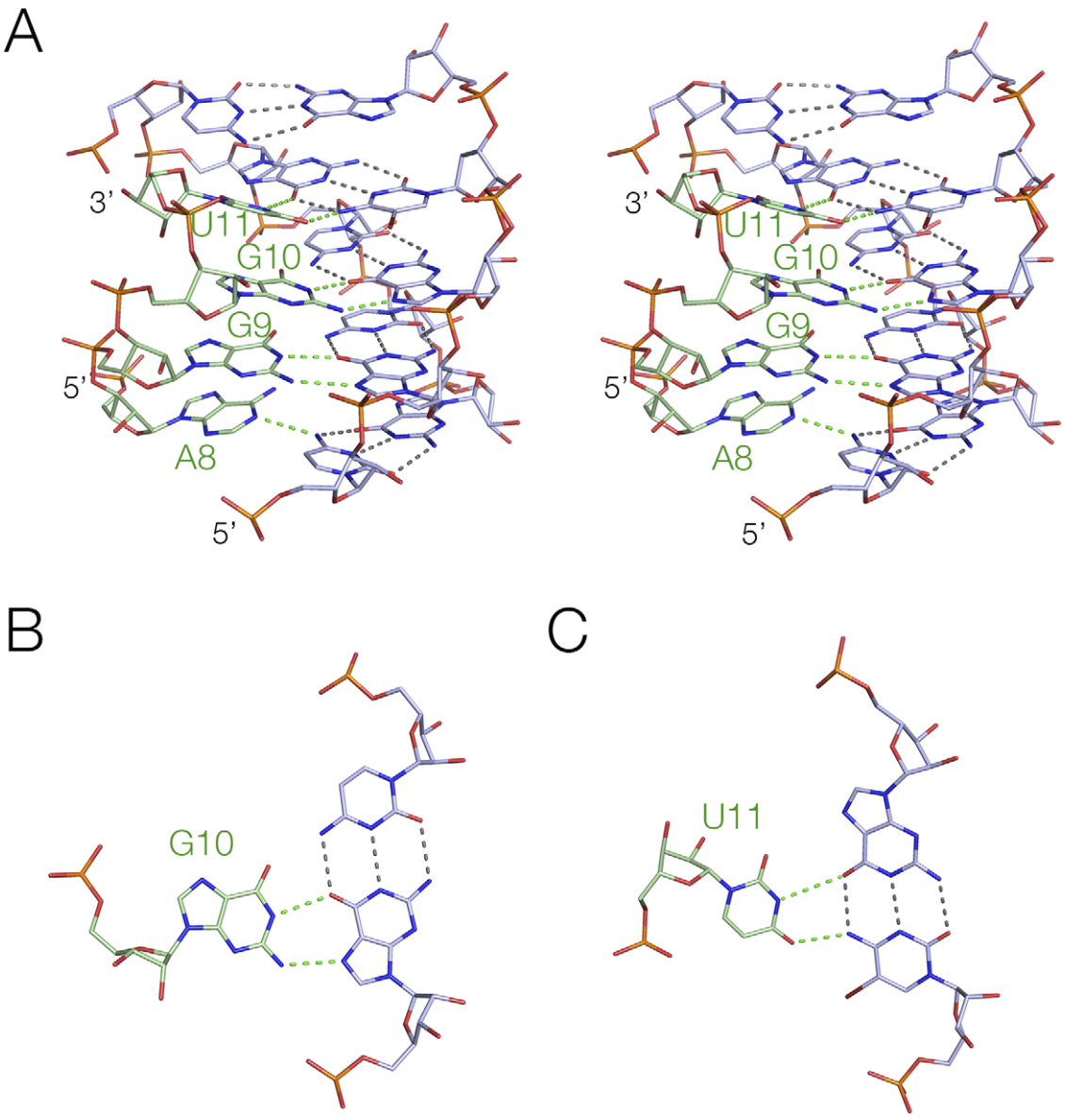

Figure 11. The major-groove triplex found in the guanidine-III riboswitch (Huang et al., 2017b). (A) Crystal structure showing the triple interaction, where the third strand is shown in green, interacting with the major groove of the duplex shown blue (PDB ID 5NWQ). (B) and (C) Structures of two triple base interactions in the major groove.

The k-junction is a combination of a three-way junction and a k-turn. This is found in the TPP riboswitches of *Arabidopsis* (Thore et al., 2006) and *E. coli* (Serganov et al., 2006), and is discussed above in the Section entitled "Three-way helical junctions". Like standard k-turns, k-junctions are also induced to fold by the addition of divalent metal ions (Li et al., 2023).

Ligand binding in riboswitches

Binding of a small-molecule ligand to a riboswitch leads to a conformational change in the RNA that in some manner modulates gene expression. As discussed earlier, in many riboswitches, the binding occurs during co-transcriptional folding of the RNA. Some riboswitches bind their ligands with high affinity (e.g., the cyclic-di-GMP-II riboswitch binds *c*-di-GMP with a K_d of 2 nM (Smith et al., 2011)), while many exhibit affinities that are lower, such as 10–100 μM range. The affinity needs to be in the range determined by the required biological response so that gene expression is altered in the required range of ligand concentration. RNA is often capable of binding ligands with higher affinities. For example, the guanidine-II riboswitch binds two guanidine molecules in separate sites with an affinity of 68 μM; when these molecules are covalently tethered, the affinity is lowered by an order of magnitude to 5 μM (Huang et al., 2019c). However, evidently in the biological context, the riboswitch needs to be sensitive to changes in guanidine concentration around 70 μM, and that is what the riboswitch has evolved to respond to.

In most cases, ultrahigh affinity is not required. Rather, binding specificity is key, and ribozymes must discriminate the biological ligand from other, potentially similar, molecules. RNA is extremely good at selective binding. RNA is a charged polymer, with hydrogen bond donors and acceptors held in a fairly rigid frame. The majority of riboswitches make multiple hydrogen bonds with their ligands. In many cases, the ligands can stack with nucleobases of the RNA.

https://doi.org/10.1017/S0033583525100012 Published online by Cambridge University Press

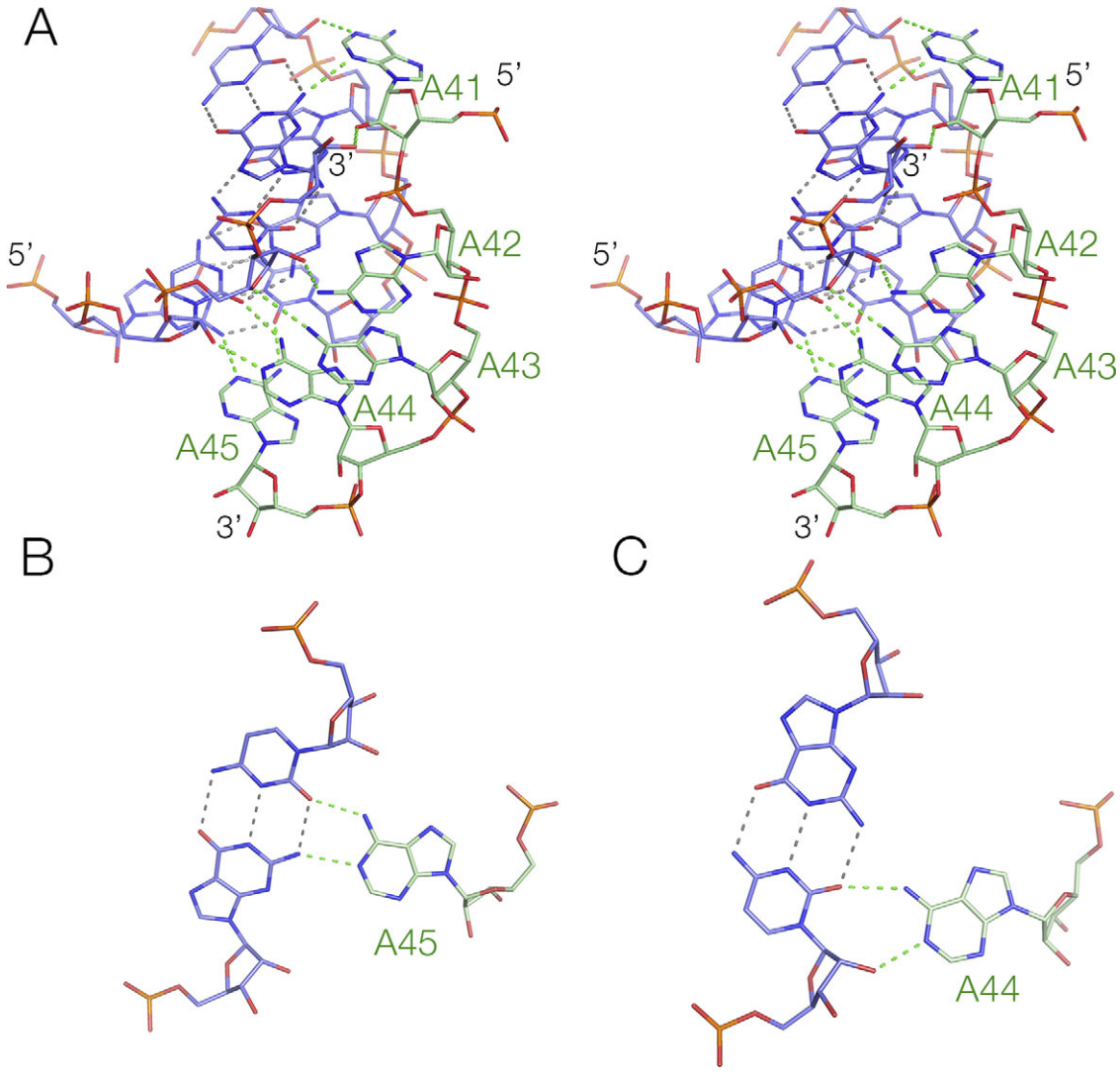

Figure 12. The minor-groove triplex found in the NAD^+-II riboswitch (Peng et al., 2023). (A) Crystal structure showing the triple interaction, where the A_n strand is shown in green, interacting with the minor groove of the duplex shown blue (PDB ID 8HB8). (B) and (C) Structures of two triple base interactions in the minor groove.

Inner-sphere metal ion interactions are found, along with cation–π interactions. All of these interactions can generate great selectivity in ligand binding.

Multiple ways a given ligand can be bound by RNA in different riboswitches

Many ligands are bound by different riboswitches, providing an opportunity to compare the manner of binding to different RNA structures. We discuss some examples of these in the following sections.

Binding of adenine-containing coenzymes to riboswitches

A number of riboswitches bind coenzymes that include nucleobases, nucleosides, or nucleotides, particularly adenosine derivatives. These often become incorporated into the riboswitch structure very much as an integral part of the RNA, base pairing with nucleobases of the RNA and stacking with nucleobases on one or both faces. This manner of binding should provide significant stabilization of the bound conformation of the RNA.

Several riboswitches bind molecules that include nucleobases, nucleosides, or nucleotides (e.g., SAM or NAD^+), and these can both hydrogen bond and stack with nucleobases of the RNA. However, the manner of base pairing varies widely. For example, the adenine of SAM base pairs as a *cis* Hoogsteen:Watson–Crick base pair with U in the SAM-I riboswitch (Montange and Batey, 2006), as a *trans* Watson–Crick:sugar base pair with G in the SAM-III riboswitch (Lu et al., 2008), and as a *trans* Hoogsteen:Watson–Crick base pair with U in the SAM-V riboswitch (Huang and Lilley, 2018b). The adenine of NAD^+ forms a Watson–Crick:sugar base pair with G in the NAD^+-I riboswitch, where it is only stacked on one face (Huang et al., 2020b), while it forms a *trans* Hoogsteen: Watson–Crick with A in the NAD^+-II riboswitch (Peng et al., 2023). The adenine of cobalamine forms a *trans* Watson–Crick: Hoogsteen base pair with A in the adenosylcobalamin (B12) riboswitch (Peselis and Serganov, 2012).

The conformation of SAM differs greatly between different SAM-binding riboswitches (Figure 14). In SAM-V, the SAM ligand is full extended along the axis of an RNA triple helix, with the adenine adopting an *anti*-conformation (Huang and Lilley, 2018b).

https://doi.org/10.1017/S0033583525100012 Published online by Cambridge University Press

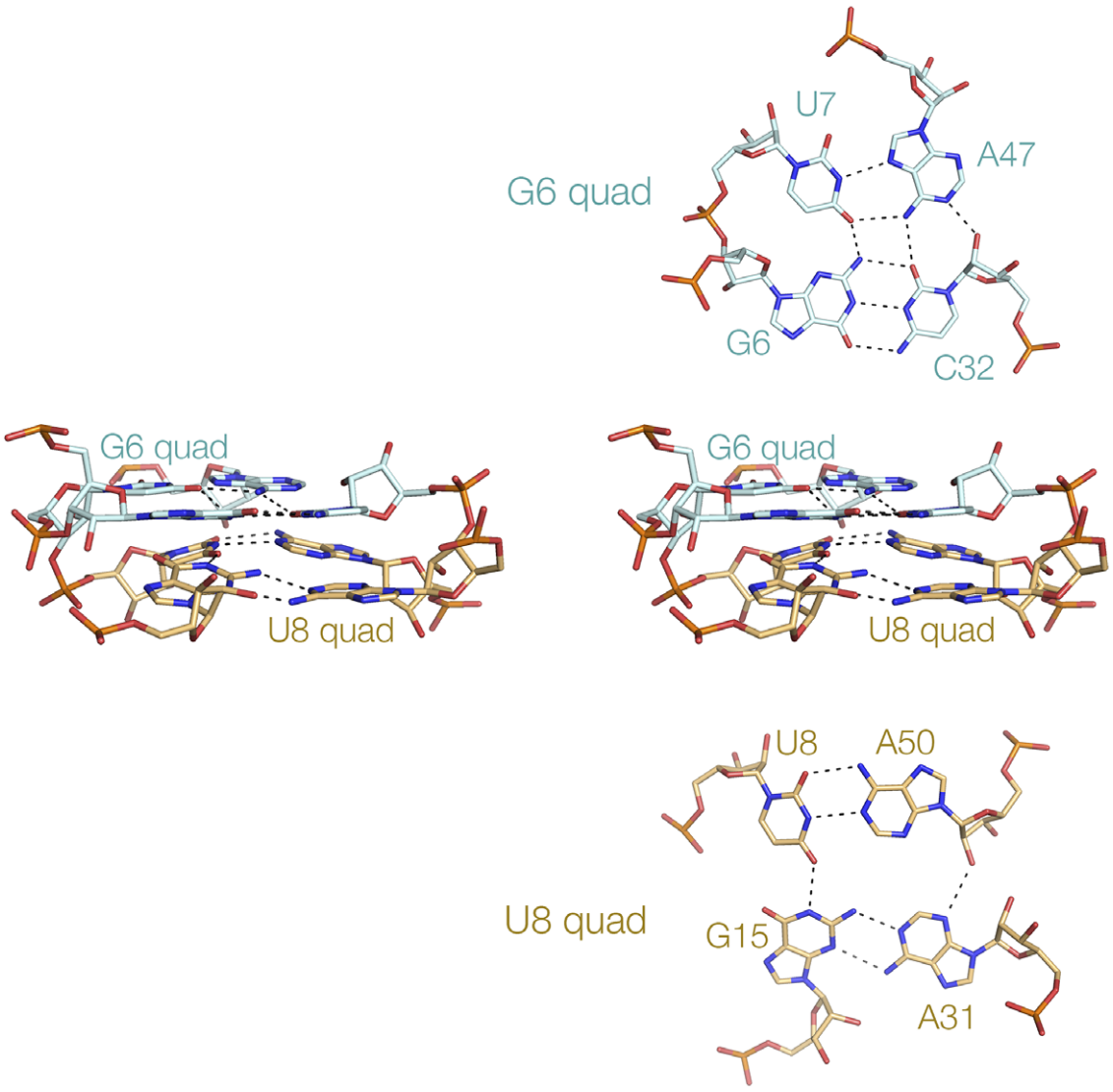

Figure 13. A tetraplex helix in the NAD^+-II riboswitch (Peng et al., 2023). This short four-stranded helix comprises two coaxial four-nucleotide tetrads. The structure is shown (center) in parallel-eye stereoscopic view, with the component G6 and U8 tetrads shown above and below, respectively (PDB ID 8HB1).

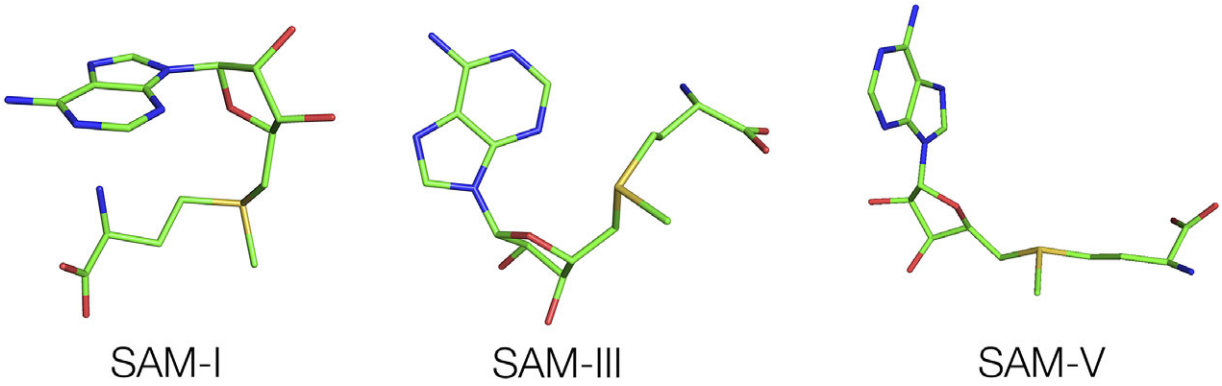

Figure 14. Various conformations of SAM observed when bound to different SAM-binding riboswitches. *Left*—Bound to the SAM-I riboswitch (Montange and Batey, 2006) (PDB ID 3GX5), *center*—bound to the SAM-III riboswitch (Lu et al., 2008) (PDB ID 3E5C), and *right*—bound to the SAM-V riboswitch (Huang and Lilley, 2018b) (PDB ID 6FZ0).

The distance between adenine N1 and the methionyl carboxylate C (N1-C) is 9.5 Å. At the other extreme, in the SAM-I riboswitch, SAM adopts an overall C-shaped conformation where the adenine adopts a *syn* conformation and the methionyl chain curves around so that the N1-C distance is 5.2 Å (Montange and Batey, 2006). This is bound in a constrained pocket formed by the minor grooves of

https://doi.org/10.1017/S0033583525100012 Published online by Cambridge University Press

two juxtaposed helices. In the SAM-III riboswitch, the methionyl chain of SAM is relatively extended but the adenine is in the *syn* conformation, with an N1-C distance of 7.1 Å (Lu et al., 2008).

These comparisons demonstrate how the different classes of SAM-binding riboswitches have evolved completely different modes of ligand binding, although SAM-II and V riboswitches are clearly very similar (Gilbert et al., 2008; Huang and Lilley, 2018b). The SAM-III and SAM-VI riboswitches were also proposed to be similar (Arachchilage et al., 2018), but this was not supported by subsequent structural analysis (Lu et al., 2008; Sun, 2019).

Binding of guanidine to riboswitches

There are three classes of guanidine-binding riboswitches. These differ in their mode of genetic control (type I exerts its control over transcriptional initiation, while types II and III control the initiation of translation) and have totally different structures (Huang et al., 2017a, 2017b; Reiss and Strobel, 2017; Reiss et al., 2017). For example, while the guanidine-II riboswitch generates two ligand binding sites by loop–loop interaction (Huang et al., 2017a; Reiss and Strobel, 2017) (see Section entitled "Loop–loop interacting structures"; Figure 10), the guanidine-III riboswitch contains a complex triple helix that includes a guanidine binding site (see Section title "PK-containing structures"; Figures 9b and 11) (Huang et al., 2017b). Yet the three riboswitches exhibit significantly common modes of ligand binding. In all three cases, the guanidine donates hydrogen bonds from two nitrogen atoms to O6 and N7 of a guanine in the RNA (Figure 15). In the guanidine-I riboswitch (Reiss et al., 2017) it is G90 that binds, while in the guanidine-II riboswitch, G9 fulfills the same role. This is the same mode of binding as some zinc finger proteins that use an arginine guanidino side chain to bind guanine in G-rich DNA (Pavletich and Pabo, 1991). In the case of the guanidine-III riboswitch, it does this twice (Huang et al., 2017b), using two different guanine nucleobases (G7 and G17). Guanidine has six protons that can be donated, and at least four are involved in hydrogen bonding to the RNA. In each case, the guanidine is stacked on a nucleobase – we return to this in Section title "Electrostatic interactions and the direct involvement of metal ions".

Few structures have been determined for riboswitches in the absence of a ligand. In a sense, this was achieved for the guanidine-II riboswitch. However, it transpired that the binding site was not really empty, but rather was occupied by three ammonium ions that took the place of the three nitrogen atoms of the guanidine ligand (Huang et al., 2017a).

Binding of adenine and nicotinamide to the NAD^+ riboswitches

The two known NAD^+-riboswitches (Malkowski et al., 2019; Panchapakesan et al., 2021) bind their NAD^+ and NADH ligands in very different ways. NAD^+ comprises adenosine and nicotinamide linked head-to-head by diphosphate (Figure 16a). In principle, either element or both could be recognized by RNA. The NAD^+-I riboswitch has two domains, with similar secondary structures composed of a long stem-loop with internal loops (Figure 16). The crystal structure of the 5′ domain (Figure 16b,c) was solved bound to AMP, ADP, ATP, NADH, NAD^+, and other derivatives (Huang et al., 2020b). In the crystal, the three helical sections are coaxially stacked, with an extended section formed by eight bulged-out nucleotides (Figure 16d). All the adenine nucleotides were observed bound to the riboswitch, but in the NADH- and NAD^+-bound forms only the adenine part was visible in the electron density. The nicotinamide was not observable, and we suspect that its binding site lies in the second domain, although no evidence in support of that has been obtained to date. The adenine moiety was observed bound under the extended bulge in an *anti*-conformation, and the whole binding site is strongly conserved. The nucleoside was coplanar with the G46:C6 base pair on its sugar edge, forming four hydrogen bonds (Figure 16e). It was stacked on one face to A8 in the bulge, while the other side was free. The binding of the diphosphate domain is metal ion mediated – this is discussed below (Section title "Electrostatic interactions and the direct involvement of metal ions").

The second NAD^+-binding riboswitch (NAD^+-II riboswitch) (Panchapakesan et al., 2021) binds principally through the nicotinamide moiety, and crystallographic structures have been determined (Peng et al., 2023; Srivastava et al., 2023). We determined the structure of the riboswitch bound to NAD^+, nicotinamide mononucleotide (NMN), and nicotinamide riboside (Peng et al., 2023). The secondary structure comprises a bulged stem-loop, with a PK formed by the ribosome binding site of the RNA (Figure 17a–c). The PK forms a triple helix (see the Section entitled "Triple helical regions" and Figure 12) that sits atop the tetraplex discussed in the Section entitled "Tetraplex helices". This forms the principal binding site for the ligand (Figure 17D). However, in contrast to the NAD^+-I riboswitch, it is the nicotinamide moiety that is bound at this site, coplanar with and sharing three hydrogen bonds to the C45:G33 base pair on its Hoogsteen edge (Figure 17e). Nicotinamide alone (as NMN) was bound at this site. NAD^+ was observed bound in an extended conformation, with the adenine bound remotely in a pocket where its nucleobase forms a single hydrogen bond to the RNA. A second binding site

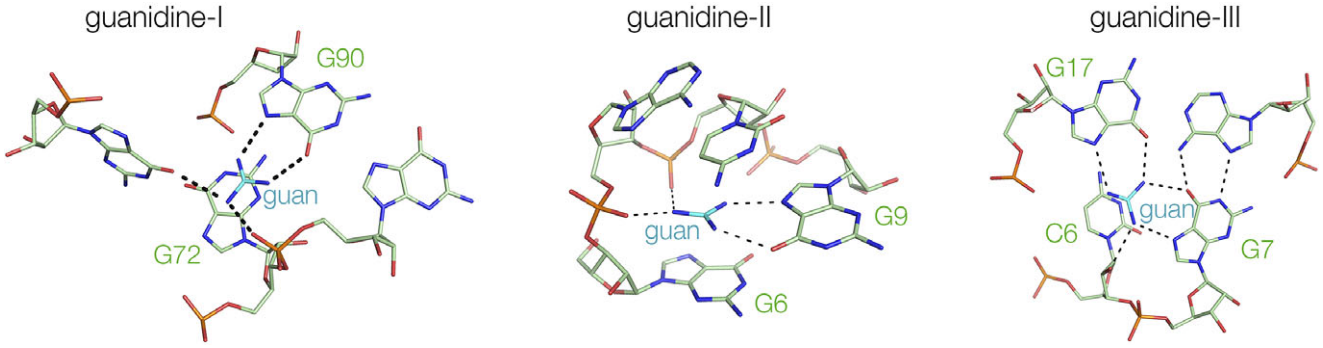

Figure 15. Comparison of the manner of guanidine binding in the guanidine I, II and III riboswitches. *Left*—bound to the guanidine-I riboswitch (Reiss et al., 2017) (PDB ID 5T83), *center*—bound to the guanidine-II riboswitch (Huang et al., 2017a) (PDB ID 5NOM) and *right*—bound to the guanidine-III riboswitch (Huang et al., 2017b) (PDB ID 5NWQ).

https://doi.org/10.1017/S0033583525100012 Published online by Cambridge University Press

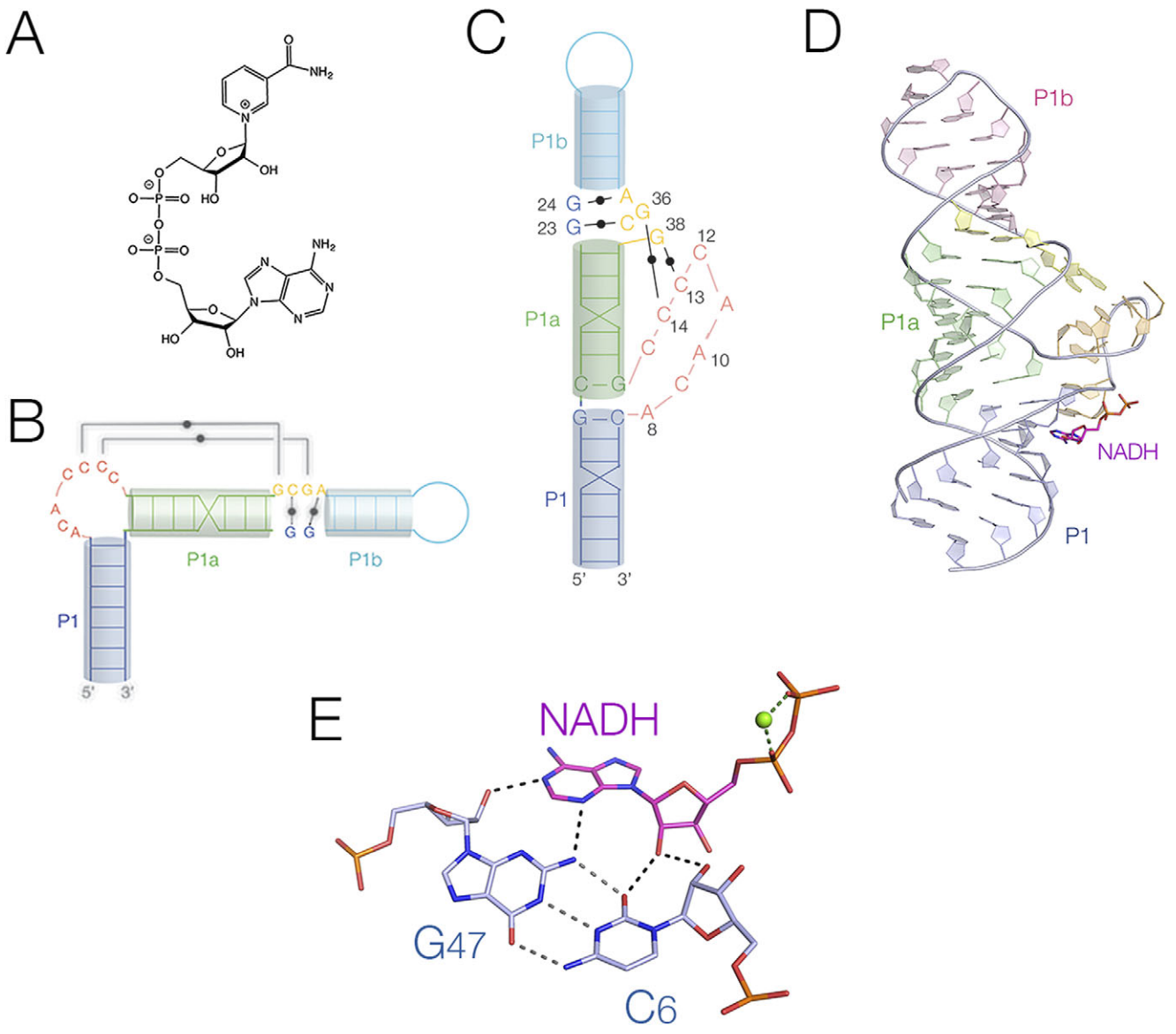

Figure 16. The binding of NADH to the NAD$^+$-I riboswitch. (A) The chemical structure of NAD$^+$. (B) Cartoon showing the secondary structure of the NAD$^+$-I riboswitch. (C) Cartoon showing the folded structure of the NAD$^+$-I riboswitch. (D) The crystal structure of the NAD$^+$-I riboswitch bound to NADH (Huang et al., 2020b) (PDB ID 6TF0). (E) The interaction between the NADH ligand and the C6:G47 base pair of the NAD$^+$-I riboswitch.

for NAD$^+$ was found in the PK helix, in which the nicotinamide was bound in pocket while the adenine end of the ligand made no specific contacts. A second structure of the NAD$^+$-II riboswitch was solved for a slightly truncated form of the RNA, where binding at a second site was not observed (Xu et al., 2023).

Binding of single versus multiple ligands by riboswitches

The majority of riboswitches bind a single ligand molecule. However, some bind two copies, either within the same RNA domain or individually to two tandem binding domains. The glycine riboswitch is an example of a tandem double riboswitch (Mandal et al., 2004). It was found that the riboswitch comprised two structured domains, and bound glycine cooperatively, in order to achieve a sharper response to rising glycine concentration by the riboswitch. The structure was determined by crystallography in the Patel and Strobel laboratories (Huang et al., 2010; Butler et al., 2011). Butler et al.'s (2011) structure confirmed that the ribozyme folded in two domains of similar structure, with inter-domain connections. These were shown to be important for the cooperative binding of glycine (Baird and Ferre-D'amare, 2013; Erion and Strobel, 2011).

The NAD$^+$-I riboswitch also appears to comprise tandemly connected domains (Malkowski et al., 2019). We solved the crystal structure of the 5′ domain, bound to a series of ligands based upon ADP, NADH and similar (Huang et al., 2020b). As discussed above (see Section entitled "Binding of adenine and nicotinamide to the NAD+ riboswitches") only the ADP moiety was observed in these structures. It was tempting to speculate that the 3′ domain might bind the nicotinamide domain, yet when Ren and coworkers (Chen et al., 2020) solved the structure of the 3′ domain they found that this also predominantly bound the ADP moiety. Nevertheless, we speculate that the tandem nature of the NAD$^+$-I riboswitch suggests a modular nature, so that by exchanging domains a different ligand might be recognized. Such as coenzyme-A, for example.

https://doi.org/10.1017/S0033583525100012 Published online by Cambridge University Press

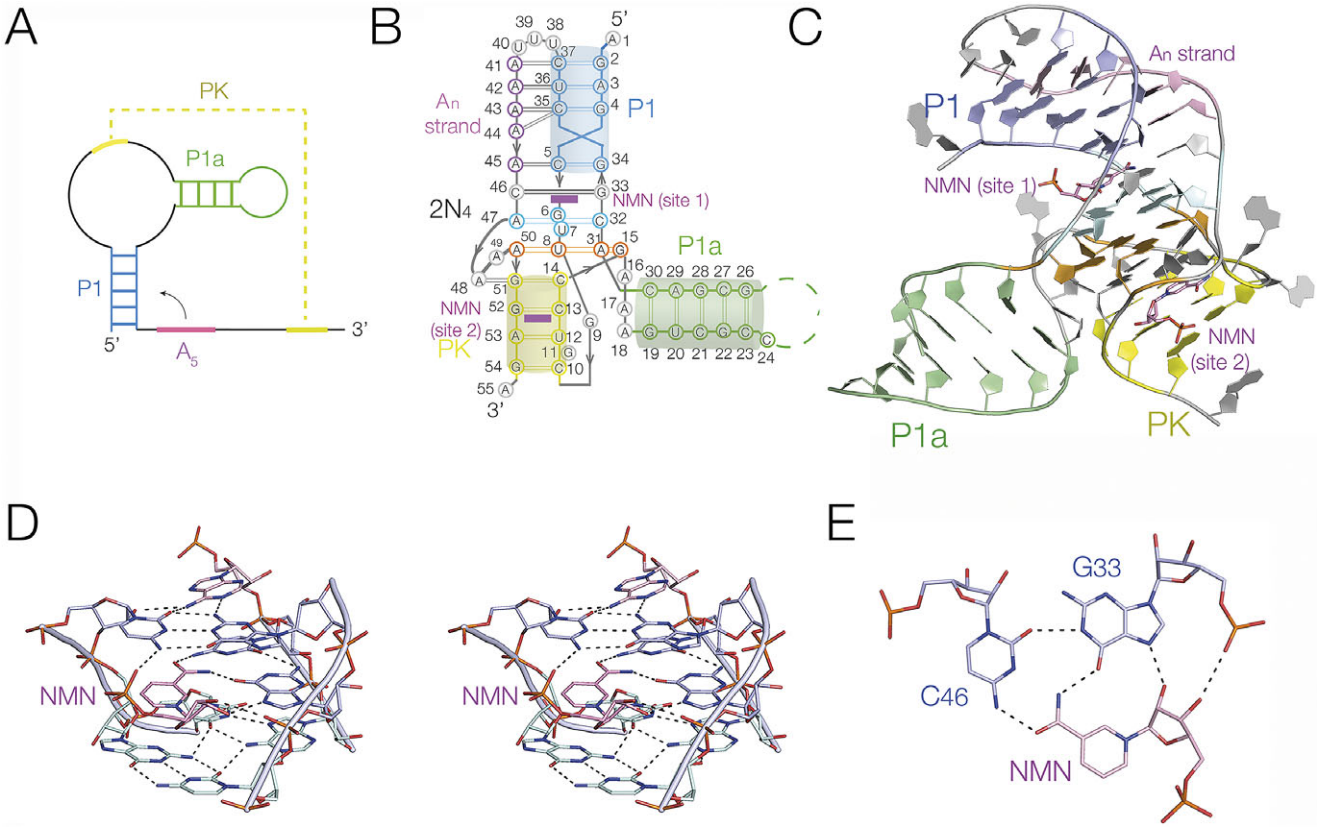

Figure 17. The binding of NMN to the NAD^+II riboswitch. (A) Scheme showing the secondary structure of the NAD^+-II riboswitch. The pseudoknot (PK, shown in yellow) forms between the internal loop and the 3′ end of the riboswitch RNA. Note that the coloring is the same in parts (a)–(c). (B) Cartoon showing the structure of the NAD^+-II riboswitch. Note that there are two molecules of NMN (shown magenta) bound at two different sites. 2N4 depicts the two quadruple base interactions; their structure is shown in Figure 13. (C) The crystal structure of the NAD^+-II riboswitch (Peng et al., 2023) (PDB ID 8HB1). (D) Detail of the structure showing the binding of NMN at site 1 shown in parallel-eye stereoscopic view. (E) The bonding interactions between the NMN ligand at site 1 and G33 and C46 of the RNA.

Some riboswitches can bind two ligand molecules within the same RNA. We have discussed the NAD^+-II riboswitch above (Section entitled "Binding of adenine and nicotinamide to the NAD^+ riboswitches"). Two molecules of NADH bind at different sites within the single riboswitch domain (Peng et al., 2023), although it is not clear whether or not binding at the second site is functionally important. The guanidine-II riboswitch also binds two molecules of guanidine within its functional unit, which is a loop–loop interaction between either closely similar tandem stem-loops, or identical ones used in crystallization (Huang et al., 2017a; Reiss and Strobel, 2017). Each of the two interacting stem-loops binds guanidine in the same manner, stabilizing the interaction. In addition, they can be covalently linked, so increasing binding affinity (Huang et al., 2019c).

Electrostatic interactions and the direct involvement of metal ions

Unlike proteins, RNA has a charged phosphodiester backbone; thus, metal ions are always involved in RNA folding processes. Most of these will be bound atmospherically without exchange of water from their inner coordination sphere, and such ions will be in rapid exchange. However, a few will undergo site binding, whereby groups from the RNA will displace inner-sphere water molecules with direct metal-RNA bonding. Such ions will be bound for much longer periods, and we frequently observe these crystallographically.

In some riboswitch-ligand co-crystal structures metal ions are observed playing a direct role in the specific binding of the ligand. In the glutamine-II riboswitch, the glutamine ligand is bound to a region of the RNA that is partially a major-groove triple helix (Huang et al., 2019b) (Figure 18A). The amide end of the glutamine forms two hydrogen bonds to the C1:G40 base pair, while the carboxylate end forms a hydrogen bond to N4 of C39. However, in addition, the other oxygen atom of the carboxylate group bonds directly to a metal ion, displacing an inner sphere water of hydration (Figure 18B). The metal ion is held in place by hydrogen bonding between other inner-sphere water molecules with the RNA. A metal ion-mediated contact of the methionyl carboxylate of SAM was found in the SAM-V riboswitch (Huang and Lilley, 2018b). Both carboxylate oxygen atoms were hydrogen bonded to the inner-sphere water molecules of a magnesium ion that was directly bonded to a backbone phosphate non-bridging oxygen atom.

Another striking example of metal ion mediated ligand binding is found in the NAD^+-I riboswitch (Huang et al., 2020b). In the structure of the NAD^+-I riboswitch (see Section entitled "Binding of adenine and nicotinamide to the NAD^+ riboswitches" and Figure 16), the neck of the loop emerging from the stacked helices is very narrow, so that the backbones approach very closely. This should generate a high local electrostatic potential, and the repulsion is diminished by binding two tightly-held divalent metal ions between the backbone phosphodiester linkages (Figure 19). Both ions are extensively dehydrated, each exchanging three

https://doi.org/10.1017/S0033583525100012 Published online by Cambridge University Press

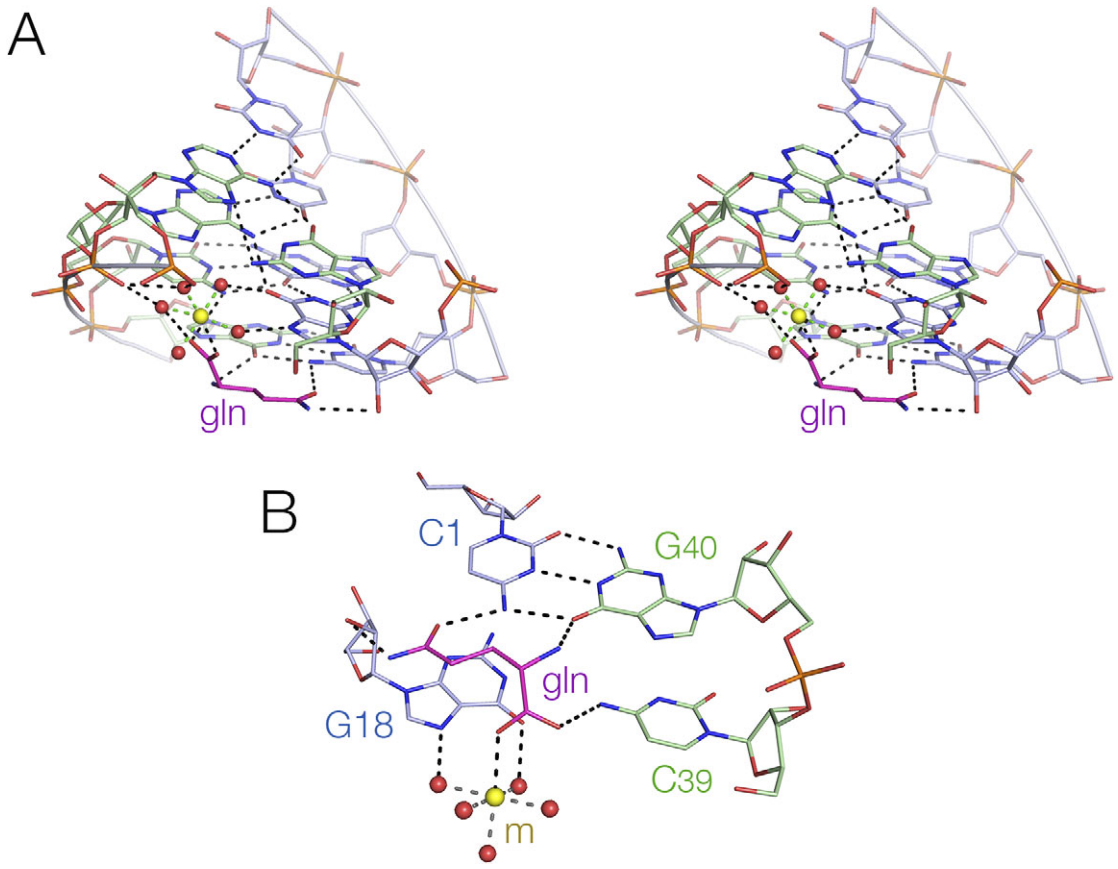

Figure 18. Metal ion-mediated binding of glutamine to the glutamine-II riboswitch. (A) The glutamine-binding domain observed in the crystal structure of the glutamine-II riboswitch (Huang et al., 2019b) shown in parallel-eye stereoscopic view. The glutamine (gln) is shown in magenta, and the metal ion is shown yellow, with red water molecules in its inner sphere of hydration (PDB ID 6QN3). (B) The bonding interactions between glutamine and the riboswitch RNA together with a hydrated magnesium ion. Note that the metal ion is directly bonded to a carboxylate oxygen of the glutamine, and that two of the inner-sphere water molecule are hydrogen bonded to G18 in the binding site.

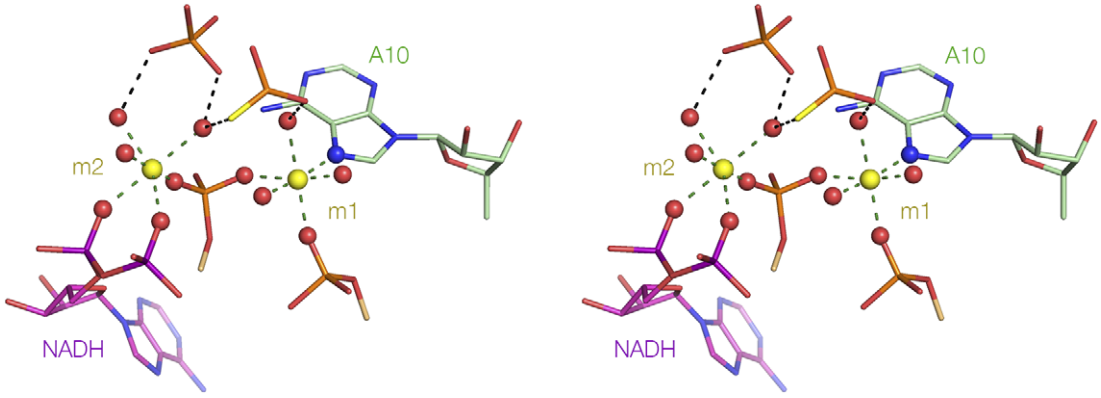

Figure 19. Metal ion-mediated binding of the diphosphate of NADH to RNA in the NAD^+-I riboswitch. The NADH is bound at the narrow neck of the extruded loop of the NAD^+-I riboswitch (refer back to Figure 16D) (Huang et al., 2020b) (PDB ID 6TF0). Two metal ions bridge the two strands of the loop at this point, shown here in parallel-eye stereoscopic view. Both ions are extensively dehydrated, forming direct bonds to the RNA or NADH ligand. In particular, we see that two non-bridging oxygen atoms are directly bonded to non-bridging oxygen atoms of the m2 metal ion.

inner-sphere water molecules for RNA ligands. Most are phosphate non-bridging oxygen atoms, but ion m1 bonds directly to N7 of A10 – such direct Mg^{2+}-N bonding is rare (Leonarski et al., 2017). Each phosphate of the diphosphate linkage of the NADH ligand makes a direct interaction with ion m2, thus making a significant contribution to the binding of the ligand to the riboswitch. In the *Arabidopsis thaliana* TPP riboswitch, the ligand diphosphate interacts with one arm of the three-way junction, with direct contacts between the non-bridging oxygen atoms of the two phosphates and magnesium ions (Thore et al., 2006).

For some riboswitches, a metal ion IS the ligand. Winkler and colleagues (Dann III et al., 2007) identified an Mg^{2+}-sensing riboswitch they termed the M-box RNA. This undergoes an Mg^{2+}-induced folding in the millimolar range. The structure was solved

https://doi.org/10.1017/S0033583525100012 Published online by Cambridge University Press

by X-ray crystallography, and the structure was found to coordinate a number of Mg^{2+}-ions, with direct Mg^{2+}-O coordination with RNA phosphate groups. Perhaps surprisingly, anion-sensing riboswitches are also known (Baker et al., 2012). Given the electronegativity of RNA, it is not immediately obvious how it would bind an anion. The crystal structure (Ren et al., 2012) showed that the folding of the riboswitch creates a pocket that binds three Mg^{2+} ions, in the middle of which binds the fluoride ion. So locally in the center of the RNA an electropositive binding pocket is created that can bind an anion. This is perhaps similar to the binding of charged phosphate groups within NAD^+ (Huang et al., 2020b) and TPP (Thore et al., 2006) discussed above, where magnesium ions mediate the interaction.

Electrostatic interactions not involving metal ions are also important. In the three guanidine riboswitch structures (Huang et al., 2017a, 2017b; Reiss and Strobel, 2017; Reiss et al., 2017), in each case, the guanidine ligand is stacked over the face of a guanine or cytosine nucleobase (Figure 15). The pK_a of guanidine is relatively high, so that at neutral pH it exists as the positively charged guanidino cation. Here, ligand binding is stabilized by a cation–π interaction. Electrostatic interactions can also be important in discriminating one ligand over another similar ligand as discussed in the following section.

Discrimination of similar ligands by riboswitches

In order for riboswitches to regulate gene expression precisely, it is vital that they discriminate their ligand from other chemically-similar molecules.

Guanidine differs from urea in that one amine of the former is replaced by a carbonyl in the latter (Figure 20a). Guanidine is highly toxic, and guanidine riboswitches control the expression of a guanidine efflux pump that detoxifies the cell (Breaker et al., 2017; Nelson et al., 2017). The regulation needs to respond to guanidine, not urea. Guanidine has three amine groups, each of which can donate two protons to hydrogen bond acceptors. The binding pocket in each guanidine riboswitch contains only hydrogen bond acceptors. There are no donors that could hydrogen bond to the carbonyl group of urea. Moreover, urea is electrically neutral at physiological pH, so there is no possibility for a cation–π interaction. This provides good discrimination between guanidine and urea in these riboswitches.

In general, the SAM-responsive riboswitches should discriminate between SAM and SAH (Figure 20b). SAH has lost the methyl group from the sulfur, which has therefore converts the positively charged sulfonium of SAM to an electrically neutral thioether. Both SAM-II and SAM-V riboswitches distinguish between SAM and SAH; for example, no evolution of heat is detectable upon the

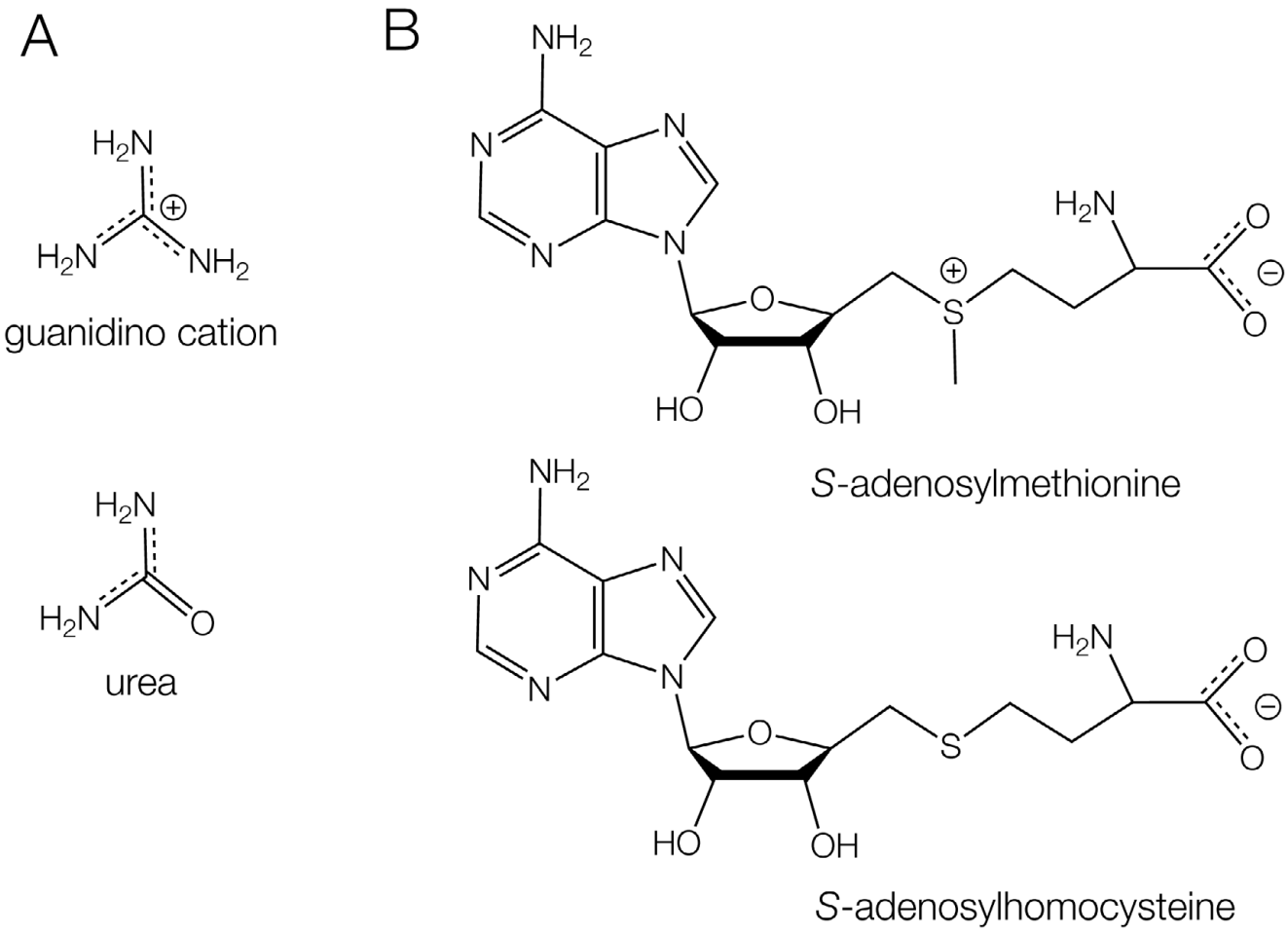

Figure 20. Comparisons of two riboswitch ligands with similar compounds that must be distinguished. (A) Guanidine (as the guanidino cation at neutral pH) compared with urea. In the latter one amine is replaced by a carbonyl, exchanging two potential hydrogen bond donors for an acceptor, and lacking the positive charge. (B) *S*-adenosylmethionine compared with *S*-adenosylhomocysteine.

https://doi.org/10.1017/S0033583525100012 Published online by Cambridge University Press

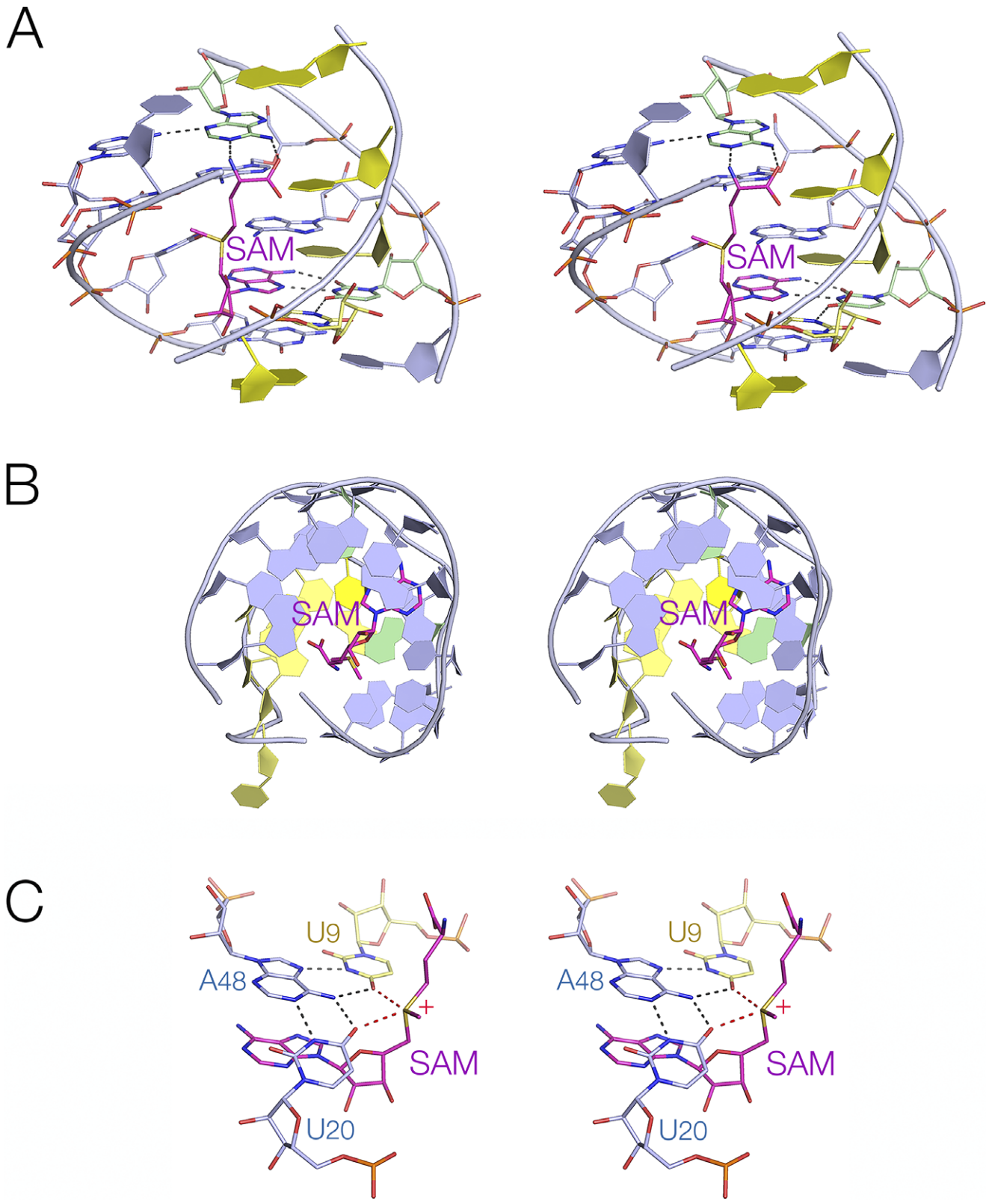

Figure 21. Electrostatic discrimination between *S*-adenosylmethionine and *S*-adenosylhomocysteine in the SAM-V riboswitch. Parallel-eye stereoscopic views are shown. (A) Side and (B) axial views of *S*-adenosylmethionine binding to the triple helical region observed in the crystal structure of the SAM-V riboswitch (Huang and Lilley, 2018b) (PDB ID 6FZ0) Note that the elongated SAM (see Figure 14) runs along the triple-helical axis. (C) The local environment of the *S*-adenosylmethionine bound to the SAM-V riboswitch. The chain extending along the axis of the triplex locates the positively charged sulfonium adjacent to the U20:A48:U9 triple such that the C4-O vectors of U20 and U9 are directed toward the sulfur. The oxygen atoms have a significant negative charge, generating an electrostatic interaction with the sulfonium ion.

https://doi.org/10.1017/S0033583525100012 Published online by Cambridge University Press

addition of SAH to the SAM-V riboswitch (Huang and Lilley, 2018b). The structure of the SAM-V riboswitch has been determined (Huang and Lilley, 2018b), which reveals the manner of SAM binding and the way it discriminates against SAH. The methyl group experiences no steric clash, so the only plausible way of distinguishing SAM from SAH is by the charge on the sulfonium group. In the riboswitch process, the SAM is bound to the triple helix (Figure 21a), and its elongated chain is extended along the axis of the triplex (Figure 21b). This places the sulfur adjacent to the U20:A48:U9 triple (Figure 21c). The C4 carbonyl groups of the two uracil nucleobases are directed toward the sulfur atom at a distance of 3.1 Å. The carbonyl oxygen atoms have a significant negative charge, and there will be an electrostatic interaction with the sulfonium in this region of low dielectric. This will not occur with a neutral SAH bound, thus providing an electrostatic mechanism for ligand discrimination. A similar mechanism of discrimination has been proposed for a similar SAM-II riboswitch (Doshi et al., 2012).

Control of translation by riboswitches

Riboswitches are ligand-responsive genetic control elements that act in *cis* in the 5′ region of mRNA to modulate gene expression. This is intimately related to RNA conformation, and changes induced by the binding of the ligand. Riboswitches can act as ON or OFF switches, although the majority act as OFF switches, downregulating gene expression when the metabolite concentration has exceeded a threshold. Riboswitches that modulate translation generally do so by alteration in RNA structure that can potentially occlude the ribosome binding site. We shall not attempt to address this topic in a comprehensive way, but rather take two examples that illustrate how this can occur, using SAM-binding riboswitches. These illustrate how a refolding of the RNA creates the ligand binding site and so becomes stabilized by the binding, and this refolding makes the ribosome binding site less accessible.

Control of translation by the SAM-V riboswitch – formation of a triple helix

The crystal structure of the SAM-V riboswitch shows the structure of the ligand-bound RNA (Huang and Lilley, 2018b). The structure is schematically depicted in Figure 22, showing that SAM binds within the triplex that forms with helix P2 (shown in Figure 21A), and thus binding of SAM should stabilize the triple helix. From bioinformatic analysis, we further proposed (Huang and Lilley, 2018b) that SAM binding leads to the stabilization of a short additional helix (P2a) located immediately 3′ to the riboswitch, and this includes part of the Shine–Dalgarno sequence. The consequence of stabilization of the triplex plus the P2a helix would be to occlude the ribosome binding site and so prevent translational initiation. Although there is no crystal structure for the ligand-free state, the structural

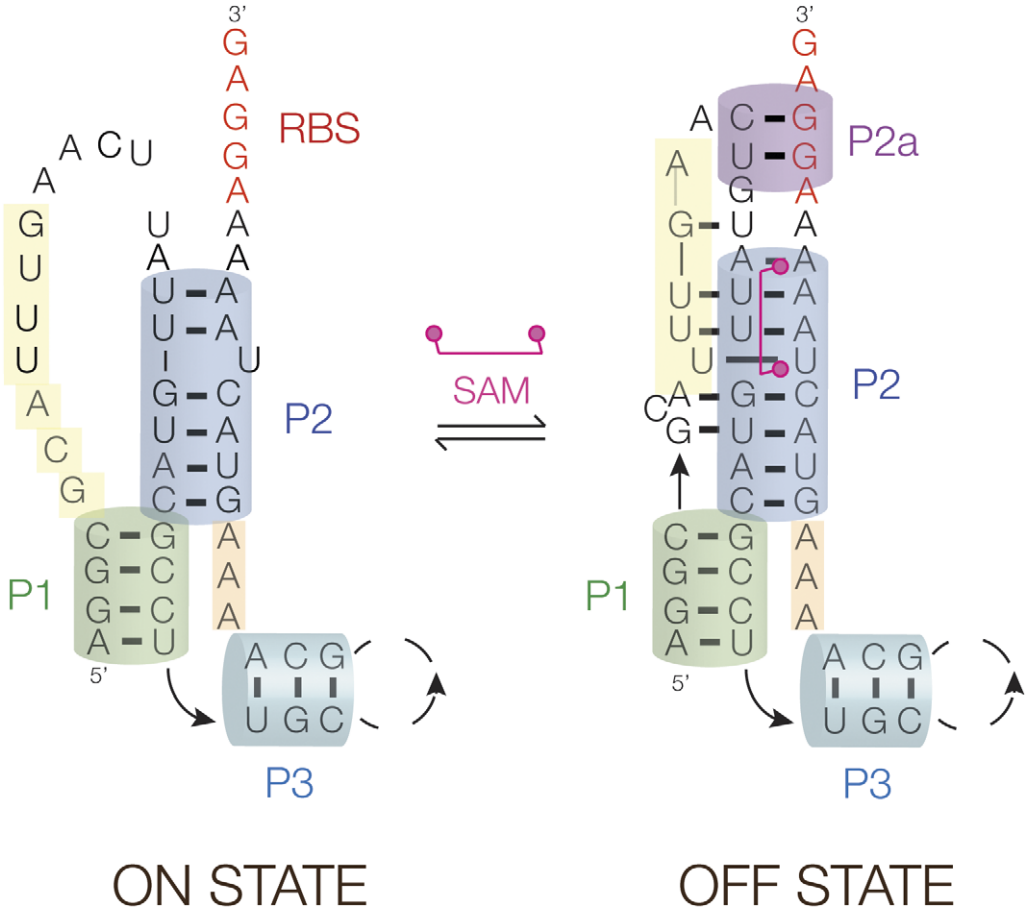

Figure 22. Translational regulation by the SAM-V riboswitch. Schematic showing the proposed mechanism for regulating the accessibility of the ribosome binding site (RBS). In the OFF state, that has the structure observed in the crystal structure (see Figure 21) (Huang and Lilley, 2018b), the bound SAM stabilizes the triple helical region plus a short duplex region (P2a) so sequestering the ribosome binding site (shown red). In-line probing data (Poiata et al., 2009) indicate that the third strand (shown yellow) disengages from the triplex with the lowering of SAM concentration, thus allowing access to the ribosome binding site and the initiation of translation.

https://doi.org/10.1017/S0033583525100012 Published online by Cambridge University Press

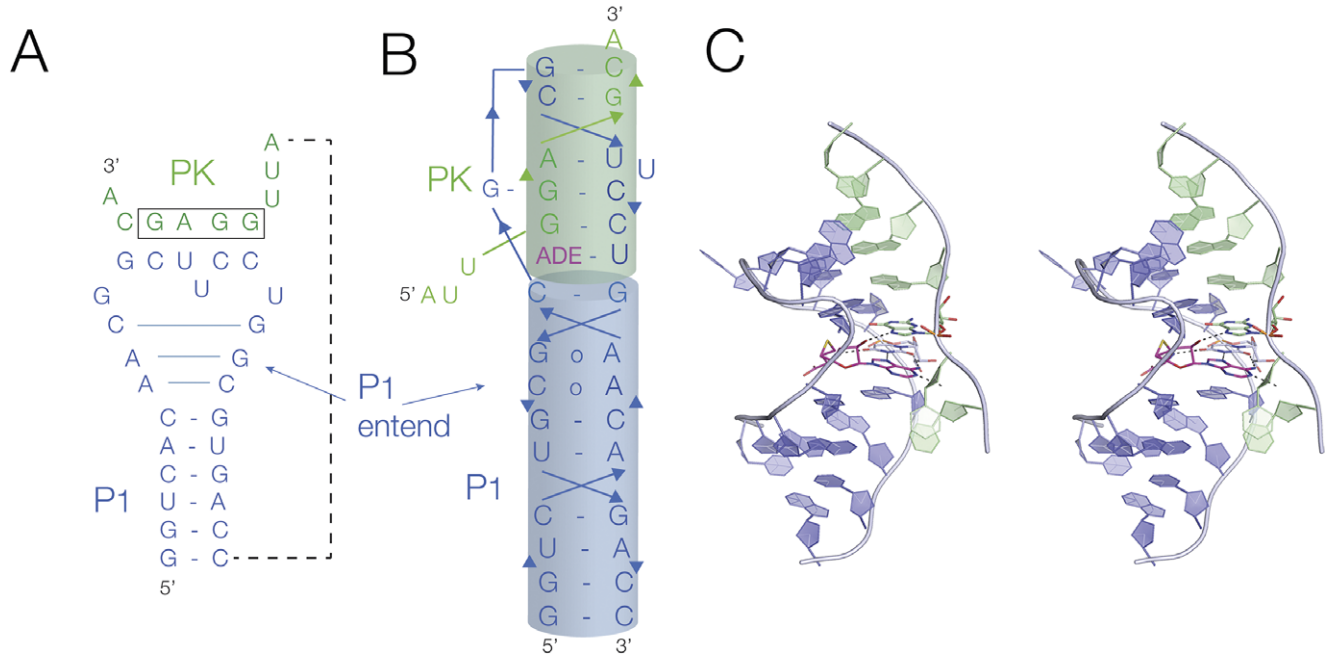

Figure 23. Translational regulation by the SAM–SAH riboswitch. (A) The secondary structure of the SAM–SAH riboswitch. In the presence of the ligand (SAM or SAH), there are two changes in conformation. The P1 helix becomes extended by three base pairs, and the pseudoknot is stabilized. The sequence forming the pseudoknot contains the ribosome binding site (boxed). (B) Cartoon of the folded structure, showing the coaxial alignment of the extended P1 and PK helices. (C) Parallel-eye stereoscopic view of the crystal structure of the SAM–SAH riboswitch with bound SAH (magenta) (Huang et al., 2020a) (PDB ID 6YL5).

transition suggested in Figure 22 involving the release of the third strand (colored yellow) in the absence of bound SAM is fully consistent with the change in the pattern of in-line probing data in the presence and absence of SAM observed by Poiata et al. (2009).

Control of translation by the SAM–SAH riboswitch – formation of a PK helix

The SAM/SAH riboswitch is overall quite similar, undergoing an SAM (or SAH)-ligand-induced conformational change that occludes the ribosome binding site in the mRNA. However, it differs in the nature of the structural change induced. In this case, the ON and OFF states differ by the formation of a ligand-stabilized PK structure (Figure 23). The ligand-induced folded structure differs in the formation of two elements, an extension of the 5′ helix (P1) by three base pairs, and the formation of the PK helix. In the crystal structure of the ligand-bound structure (Huang et al., 2020a), the PK helix is coaxial with the extended P1 helix, and the SAM or SAH ligand is bound at the interface between the two. Single molecule experiments showed that either SAM or SAH stabilizes the folded form with the PK helix stabilized (Huang et al., 2020a; Liao et al., 2023). Since the ribosome binding site is contained within the PK helix it is clear that this would be occluded by ligand-induced folding. This was demonstrated by studying the accessibility to oligonucleotides that should mimic the ribosome binding site (Liao et al., 2023).

These two examples show how intimately connected ligand binding and structural rearrangement into a conformation that prevents access to the ribosome binding site are. Therefore, in these riboswitches at least, the commonly used division of riboswitches into an aptamer (ligand binding) domain, and an expression platform (where the genetic control is mediated) is not really applicable.

Conclusion

Near-atomic resolution structures have been determined for most classes of riboswitch, and this has provided a valuable database of RNA structure that can be mined for general insights into RNA conformation and folding. Moreover, the riboswitches specifically bind a wide variety of a small-molecule ligand, thus yielding a general understanding of RNA–ligand interactions.

For the most part, riboswitches are relatively small RNA molecules, folding as a single domain. We see that frequently these are based upon a single structural element such as a helical junction or PK. In addition, some structural elements recur through the ensemble of riboswitch structures, particularly elements such as triple helical sections, loop–loop and loop–receptor interactions, and k-turns and junctions.

In general, it is these elements that create ligand binding sites in the RNA, binding with great specificity, and discriminating against similar related molecules. The riboswitches exhibit multiple ways to bind their ligands, and the same ligand (e.g., SAM) can be bound in different ways in different riboswitches. The ligand can become intimately assimilated into the RNA structure, almost to become part of the RNA. Adenosine-containing ligands form base pairs with the RNA, being both hydrogen bonded and stacked just like a section of the RNA itself. Electrostatic interactions can be important, and metal-ion-mediated contacts are frequently found.

The binding of a ligand into local structural elements stabilizes the structure, and that is often the key to how the riboswitch functions. In the translational riboswitches, the ligand-bound structure generally occludes the ribosome binding site, so preventing ribosomal access and, thus, the initiation of translation.

Study of the riboswitches teaches us much about the RNA structure, ligand binding, and how these combine to regulate gene expression.

https://doi.org/10.1017/S0033583525100012 Published online by Cambridge University Press

Acknowledgments. The authors would like to thank Dr Timothy Wilson for discussion.

Financial support. Riboswitch work has been funded in Dundee by Cancer Research UK (program grant A18604) and in Guangzhou by the National Natural Science Foundation of China (32171191) and Guangdong Science and Technology Department (2024A1515012594, 2023B1212060013, and 2020B1212030004).

Competing interests. The authors declare no conflict of interest.

References

Ames TD and Breaker RR (2011) Bacterial aptamers that selectively bind glutamine. *RNA Biology* **8**(1), 82–89.

Arachchilage GM *et al.* (2018) SAM-VI RNAs selectively bind S-adenosylmethionine and exhibit similarities to SAM-III riboswitches. *RNA Biology* **15**(3), 371–378.

Baird NJ and Ferre-D'amare AR (2013) Modulation of quaternary structure and enhancement of ligand binding by the K-turn of tandem glycine riboswitches. *RNA* **19**(2), 167–176.

Baker JL *et al.* (2012) Widespread genetic switches and toxicity resistance proteins for fluoride. *Science* **335**(6065), 233–235.

Batey RT *et al.* (2004) Structure of a natural guanine-responsive riboswitch complexed with the metabolite hypoxanthine. *Nature* **432**(7015), 411–415.

Blouin S and Lafontaine DA (2007) A loop interaction and a K-turn motif located in the lysine aptamer domain are important for the riboswitch gene regulation control. *RNA* **13**(8), 1256–12567.

Breaker RR (2012) Riboswitches and the RNA world. *Cold Spring Harbor Perspectives in Biology* **4**(2), a003566.

Breaker RR *et al.* (2017) The biology of free guanidine as revealed by riboswitches. *Biochemistry* **56**(2), 345–347.

Bu F *et al.* (2024) Ribocentre-switch: A database of riboswitches. *Nucleic Acids Research* **52**(D1), D265–D272.

Butler EB *et al.* (2011) Structural basis of cooperative ligand binding by the glycine riboswitch. *Chemistry & Biology* **18**(3), 293–298.

Cheah MT *et al.* (2007) Control of alternative RNA splicing and gene expression by eukaryotic riboswitches. *Nature* **447**(7143), 497–500.

Chen H *et al.* (2020) Structural distinctions between NAD^+ riboswitch domains 1 and 2 determine differential folding and ligand binding. *Nucleic Acids Research* **48**(21), 12394–12406.

Cochrane JC *et al.* (2007) Structural investigation of the GlmS ribozyme bound to its catalytic cofactor. *Chemistry & Biology* **14**, 97–105.

Connelly CM *et al.* (2019) Synthetic ligands for PreQ(1) riboswitches provide structural and mechanistic insights into targeting RNA tertiary structure. *Nature Communications* **10**(1), 1501.

Dambach M *et al.* (2015) The ubiquitous yybP-ykoY riboswitch is a manganese-responsive regulatory element. *Molec. Cell* **57**(6), 1099–1109.

Dann III CE *et al.* (2007) Structure and mechanism of a metal-sensing regulatory RNA. *Cell* **130**(5), 878–892.

Daume M *et al.* (2017) RIP-Seq suggests translational regulation by L7Ae in archaea. *MBio* **8**(4), e00730-17.

Doshi U *et al.* (2012) Atomic-level insights into metabolite recognition and specificity of the SAM-II riboswitch. *RNA* **18**(2), 300–307.

Duckett DR *et al.* (1988) The structure of the Holliday junction and its resolution. *Cell* **55**, 79–89.

Duckett DR *et al.* (1995) The global folding of four-way helical junctions in RNA, including that in U1 snRNA. *Cell* **83**, 1027–1036.

Erion TV and Strobel SA (2011) Identification of a tertiary interaction important for cooperative ligand binding by the glycine riboswitch. *RNA* **17**(1), 74–84.

Frieda KL and Block SM (2012) Direct observation of cotranscriptional folding in an adenine riboswitch. *Science* **338**(6105), 397–400.

Furukawa K *et al.* (2015) Bacterial riboswitches cooperatively bind Ni^{2+} or Co^{2+} ions and control expression of heavy metal transporters. *Molecular Cell* **57**(6), 1088–1098.

Garst AD *et al.* (2008) Crystal structure of the lysine riboswitch regulatory mRNA element. *The Journal of Biological Chemistry* **283**(33), 22347–22351.

Gilbert SD *et al.* (2008) Structure of the SAM-II riboswitch bound to S-adenosylmethionine. *Nature Structural & Molecular Biology* **15**(2), 177–182.

Goody TA *et al.* (2004) The kink-turn motif in RNA is dimorphic, and metal ion dependent. *RNA* **10**, 254–264.

Grundy FJ *et al.* (2003) The L box regulon: Lysine sensing by leader RNAs of bacterial lysine biosynthesis genes. *Proceedings of the National Academy of Sciences of the United States of America* **100**(21), 12057–12062.

Henkin TM *et al.* (1992) Analysis of the *Bacillus subtilis* tyrS gene: Conservation of a regulatory sequence in multiple tRNA synthetase genes. *Journal of Bacteriology* **174**(4), 1299–1306.

Hohng S *et al.* (2004) Conformational flexibility of four-way junctions in RNA. J. *Molecular Biology* **336**, 69–79.

Hua B *et al.* (2020) Real-time monitoring of single ZTP riboswitches reveals a complex and kinetically controlled decision landscape. *Nature Communications* **11**(1), 4531.

Huang L and Lilley DMJ (2013) The molecular recognition of kink-turn structure by the L7Ae class of proteins. *RNA* **19**(12), 1703–1710.

Huang L and Lilley DMJ (2016) The kink turn, a key architectural element in RNA structure. *Journal of Molecular Biology* **428**(5 Pt A), 790–801.

Huang L and Lilley DMJ (2018a) The kink-turn in the structural biology of RNA. *Quarterly Reviews of Biophysics* **51**, e5.

Huang L and Lilley DMJ (2018b) Structure and ligand binding of the SAM-V riboswitch. *Nucleic Acids Research* **46**, 6869–6879.

Huang L *et al.* (2010) Structural insights into ligand recognition by a sensing domain of the cooperative glycine riboswitch. *Molecular Cell* **40**(5), 774–786.

Huang L *et al.* (2016) A critical base pair in k-turns determines the conformational class adopted, and correlates with biological function. *Nucleic Acids Research* **44**(11), 5390–5398.

Huang L *et al.* (2017a) The structure of the guanidine-II riboswitch. *Cell Chemical Biology* **24**, 695–702.

Huang L *et al.* (2017b) Structure of the guanidine III riboswitch. *Cell Chemical Biology* **24**(11), 1407–1415.

Huang L *et al.* (2019a) The role of RNA structure in translational regulation by L7Ae protein in archaea. *RNA* **25**(1), 60–69.

Huang L *et al.* (2019b) Structure and ligand binding of the glutamine-II riboswitch. *Nucleic Acids Research* **47**, 7666–7675.

Huang L *et al.* (2019c) Structure-guided design of a high affinity ligand for a riboswitch. *RNA* **25**, 423–430.

Huang L *et al.* (2020a) Crystal structure and ligand-induced folding of the SAM/SAH riboswitch. *Nucleic Acids Research* **48**(13), 7545–7556.

Huang L *et al.* (2020b) Structure and ligand binding of the ADP-binding domain of the NAD^+ riboswitch. *RNA* **26**(7), 878–887.

Johnson Jr JE *et al.* (2012) B12 cofactors directly stabilize an mRNA regulatory switch. *Nature* **492**(7427), 133–137.

Kavita K and Breaker RR (2023) Discovering riboswitches: The past and the future. *Trends in Biochemical Sciences* **48**(2), 119–141.

Klein DJ and Ferré-D'amaré AR (2006) Structural basis of glmS ribozyme activation by glucosamine-6-phosphate. *Science* **313**(5794), 1752–1756.

Klein DJ *et al.* (2001) The kink-turn: A new RNA secondary structure motif. *The EMBO Journal* **20**(15), 4214–4221.

Knappenberger AJ *et al.* (2018) Structures of two aptamers with differing ligand specificity reveal ruggedness in the functional landscape of RNA. *eLife* **7**, e36381.

Lemay J-F *et al.* (2006) Folding of the adenine riboswitch. *Chemistry & Biology* **13**, 857–868.

Leonarski F *et al.* (2017) Mg^{2+} ions: Do they bind to nucleobase nitrogens? *Nucleic Acids Research* **45**(2), 987–1004.

Lescoute A and Westhof E (2006) Topology of three-way junctions in folded RNAs. *RNA* **12**(1), 83–93.

Li M *et al.* (2023) Structure and ion-dependent folding of k-junctions. *RNA* **29**(9), 1411–1422.

Liao TW *et al.* (2023) Linking folding dynamics and function of SAM/SAH riboswitches at the single molecule level. *Nucleic Acids Research* **51**(17), 8957–8969.

Liberman JA *et al.* (2013) Structure of a class II preQ1 riboswitch reveals ligand recognition by a new fold. *Nature Chemical Biology* **9**(6), 353–355.

Lilley DMJ *et al.* (1995) Nomenclature Committee of the International Union of biochemistry: A nomenclature of junctions and branchpoints in nucleic acids. Recommendations 1994. *European Journal of Biochemistry* **230**, 1–2.

https://doi.org/10.1017/S0033583525100012 Published online by Cambridge University Press

Liu J and Lilley DMJ (2007) The role of specific 2′-hydroxyl groups in the stabilization of the folded conformation of kink-turn RNA. *RNA* **13**(2), 200–210.

Lu C *et al.* (2008) Crystal structures of the SAM-III/S(MK) riboswitch reveal the SAM-dependent translation inhibition mechanism. *Nature Structural & Molecular Biology* **15**(10), 1076–1083.

Malkowski SN *et al.* (2019) Evidence that the nadA motif is a bacterial riboswitch for the ubiquitous enzyme cofactor NAD^+. *RNA* **25**, 1616–1627.

Mandal M *et al.* (2004) A glycine-dependent riboswitch that uses cooperative binding to control gene expression. *Science* **306**(5694), 275–279.

Matyjasik MM and Batey RT (2019) Structural basis for 2′-deoxyguanosine recognition by the 2′-dG-II class of riboswitches. *Nucleic Acids Research* **47**(20), 10931–10941.

Mccown PJ *et al.* (2017) Riboswitch diversity and distribution. *RNA* **23**(7), 995–1011.

Mckinney SA *et al.* (2003) Structural dynamics of individual Holliday junctions. *Nature Structural Biology* **10**(2), 93–97.

Mcphee SA *et al.* (2014) A critical base pair in k-turns that confers folding characteristics and correlates with biological function. *Nature Communications* **5**, 5127.

Montange RK and Batey RT (2006) Structure of the S-adenosylmethionine riboswitch regulatory mRNA element. *Nature* **441**(7097), 1172–1175.

Moore T *et al.* (2004) Molecular basis of box C/D RNA-protein interactions; Cocrystal structure of archaeal L7Ae and a box C/D RNA. *Structure* **12**(5), 807–818.

Murchie, A. I. H., Clegg, R. M., Von Kitzing, E., Duckett, D. R., Diekmann, S. & Lilley, D. M. J. (1989). Fluorescence energy transfer shows that the four-way DNA junction is a right-handed cross of antiparallel molecules. *Nature*, **341**, 763–766.

Nelson JW *et al.* (2017) Metabolism of free guanidine in bacteria is regulated by a widespread riboswitch class. *Molecular Cell* **65**(2), 220–230.

Nissen P *et al.* (2001) RNA tertiary interactions in the large ribosomal subunit: The A-minor motif. *Proceedings of the National Academy of Sciences of the United States of America* **98**, 4899–4903.

Olenginski LT *et al.* (2024) Flipping the script: Understanding riboswitches from an alternative perspective. *The Journal of Biological Chemistry* **300**(3), 105730.

Ouellet J *et al.* (2010) Structure of the three-way helical junction of the hepatitis C virus IRES element. *RNA* **16**(8), 1597–1609.

Panchapakesan SSS *et al.* (2021) A second riboswitch class for the enzyme cofactor NAD^+. *RNA* **27**(1), 99–105.

Pavletich NP and Pabo CO (1991) Zinc finger-DNA recognition: Crystal structure of a Zif268-DNA complex at 2.1 Å. *Science* **252**, 809–817.

Peng X *et al.* (2023) Crystal structures of the NAD^+-II riboswitch reveal two distinct ligand-binding pockets. *Nucleic Acids Research* **51**(6), 2904–2914.

Peselis A and Serganov A (2012) Structural insights into ligand binding and gene expression control by an adenosylcobalamin riboswitch. *Nature Structural & Molecular Biology* **19**(11), 1182–1184.

Pikovskaya O *et al.* (2011) Structural principles of nucleoside selectivity in a 2′-deoxyguanosine riboswitch. *Nature Chemical Biology* **7**(10), 748–755.

Poiata E *et al.* (2009) A variant riboswitch aptamer class for S-adenosylmethionine common in marine bacteria. *RNA* **15**(11), 2046–2056.

Price IR *et al.* (2015) Mn^{2+}-sensing mechanisms of yybP-ykoY orphan riboswitches. *Molecular Cell* **57**(6), 1110–1123.

Ramesh A *et al.* (2011) Insights into metalloregulation by M-box riboswitch RNAs via structural analysis of manganese-bound complexes. *Journal of Molecular Biology* **407**(4), 556–570.

Reiss CW and Strobel SA (2017) Structural basis for ligand binding to the guanidine-II riboswitch. *RNA* **23**(9), 1338–1343.

Reiss CW *et al.* (2017) Structural basis for ligand binding to the guanidine-I riboswitch. *Structure* **25**(1), 195–202.

Ren A *et al.* (2012) Fluoride ion encapsulation by Mg^{2+} ions and phosphates in a fluoride riboswitch. *Nature* **486**(7401), 85–89.

Ren A *et al.* (2015a) Structural basis for molecular discrimination by a 3′,3’-cGAMP sensing riboswitch. *Cell Reports* **11**(1), 1–12.

Ren A *et al.* (2015b) Structural and dynamic basis for low-affinity, high-selectivity binding of L-glutamine by the glutamine riboswitch. *Cell Reports* **13**(9), 1800–1813.

Schroeder GM *et al.* (2023) Structure and function analysis of a type III preQ1-I riboswitch from *Escherichia coli* reveals direct metabolite sensing by the Shine-Dalgarno sequence. *The Journal of Biological Chemistry* **299**(10), 105208.

Schroeder KT *et al.* (2011) RNA tertiary interactions in a riboswitch stabilize the structure of a kink turn. *Structure* **19**(9), 1233–1240.

Serganov A *et al.* (2004) Structural basis for discriminative regulation of gene expression by adenine- and guanine-sensing mRNAs. *Chemistry & Biology* **11**(12), 1729–1741.

Serganov A *et al.* (2006) Structural basis for gene regulation by a thiamine pyrophosphate-sensing riboswitch. *Nature* **441**(7097), 1167–1171.

Serganov A *et al.* (2008) Structural insights into amino acid binding and gene control by a lysine riboswitch. *Nature* **455**(7217), 1263–1267.

Sherlock ME *et al.* (2017) Biochemical validation of a second guanidine riboswitch class in bacteria. *Biochemistry* **56**(2), 352–358.

Smith KD *et al.* (2009) Structural basis of ligand binding by a c-di-GMP riboswitch. *Nature Structural & Molecular Biology* **16**(12), 1218–1223.

Smith KD *et al.* (2011) Structural basis of differential ligand recognition by two classes of bis-(3′-5′)-cyclic dimeric guanosine monophosphate-binding riboswitches. *Proceedings of the National Academy of Sciences of the United States of America* **108**, 7757–7762.

Srivastava Y *et al.* (2023) Full-length NAD^+-I riboswitches bind a single cofactor but cannot discriminate against adenosine triphosphate. *Biochemistry* **62**(23), 3396–3410.

Sudarsan N *et al.* (2003) An mRNA structure in bacteria that controls gene expression by binding lysine. *Genes & Development* **17**(21), 2688–2697.

Sun, A. *et al* (2019) SAM-VI riboswitch structure and signature for ligand discrimination. *Nature communications* **10**, 5728.

Thore S *et al.* (2006) Structure of the eukaryotic thiamine pyrophosphate riboswitch with its regulatory ligand. *Science* **312**(5777), 1208–1211.

Trausch JJ *et al.* (2011) The structure of a tetrahydrofolate-sensing riboswitch reveals two ligand binding sites in a single aptamer. *Structure* **19**(10), 1413–1423.

Turner B and Lilley DMJ (2008) The importance of G.A hydrogen bonding in the metal ion- and protein-induced folding of a kink turn RNA. J. *Molecular Biology* **381**(2), 431–442.

Vidovic I *et al.* (2000) Crystal structure of the spliceosomal 15.5 kD protein bound to a U4 snRNA fragment. *Molecular Cell* **6**(6), 1331–1342.

Wang J *et al.* (2012) Single-molecule observation of the induction of k-turn RNA structure on binding L7Ae protein. *Biophysical Journal* **103**(12), 2541–2548.

Wang J *et al.* (2014) The k-junction motif in RNA structure. *Nucleic Acids Research* **42**(8), 5322–5331.

Wickiser JK *et al.* (2005) The speed of RNA transcription and metabolite binding kinetics operate an FMN riboswitch. *Molecular Cell* **18**(1), 49–60.

Widom JR, Nedialkov YA, Rai V, Hayes RL, Brooks III CL, Artsimovitch I and Walter NG (2018) Ligand modulates cross-coupling between riboswitch folding and transcriptional pausing. *Molecular Cell* **72**(3), 541–552; e546.

Winkler W *et al.* (2002) Thiamine derivatives bind messenger RNAs directly to regulate bacterial gene expression. *Nature* **419**(6910), 952–956.

Winkler WC *et al.* (2004) Control of gene expression by a natural metabolite-responsive ribozyme. *Nature* **428**(6980), 281–286.

Xu X *et al.* (2023) Structure-based investigations of the NAD^+-II riboswitch. *Nucleic Acids Research* **51**(1), 54–67.

Zhang J and Ferre-D’amare AR (2013) Co-crystal structure of a T-box riboswitch stem I domain in complex with its cognate tRNA. *Nature* **500**(7462), 363–366.

https://doi.org/10.1017/S0033583525100012 Published online by Cambridge University Press